The Abdus Salam
International Centre for Theoretical Physics

United Nations
Educational, Scientific and
Cultural Organization

IAEA
International Atomic Energy Agency

2022-17

Workshop on Theoretical Ecology and Global Change

2 - 18 March 2009

Mechanistic scaling of ecosystem function and dynamics in space and time: Ecosystem Demography model version 2

MOORCROFT Paul
Harvard University
Department of Organismic and Evolutionary Biology
26 Oxford Street, 02138 MA Cambridge
U.S.A.

JOURNAL OF GEOPHYSICAL RESEARCH, VOL. 114, G01002, doi:10.1029/2008JG000812, 2009

Mechanistic scaling of ecosystem function and dynamics in space and time: Ecosystem Demography model version 2

D. Medvigy,[1,2] S. C. Wofsy,[3] J. W. Munger,[3] D. Y. Hollinger,[4] and P. R. Moorcroft[5]

Received 1 July 2008; revised 5 October 2008; accepted 20 October 2008; published 17 January 2009.

[1] Insights into how terrestrial ecosystems affect the Earth's response to changes in climate and rising atmospheric CO_2 levels rely heavily on the predictions of terrestrial biosphere models (TBMs). These models contain detailed mechanistic representations of biological processes affecting terrestrial ecosystems; however, their ability to simultaneously predict field-based measurements of terrestrial vegetation dynamics and carbon fluxes has remained largely untested. In this study, we address this issue by developing a constrained implementation of a new structured TBM, the Ecosystem Demography model version 2 (ED2), which explicitly tracks the dynamics of fine-scale ecosystem structure and function. Carbon and water flux measurements from an eddy-flux tower are used in conjunction with forest inventory measurements of tree growth and mortality at Harvard Forest (42.5°N, 72.1°W) to estimate a number of important but weakly constrained model parameters. Evaluation against a decade of tower flux and forest dynamics measurements shows that the constrained ED2 model yields greatly improved predictions of annual net ecosystem productivity, carbon partitioning, and growth and mortality dynamics of both hardwood and conifer trees. The generality of the model formulation is then evaluated by comparing the model's predictions against measurements from two other eddy-flux towers and forest inventories of the northeastern United States and Quebec. Despite the markedly different composition throughout this region, the optimized model realistically predicts observed patterns of carbon fluxes and tree growth. These results demonstrate how TBMs parameterized with field-based measurements can provide quantitative insight into the underlying biological processes governing ecosystem composition, structure, and function at larger scales.

Citation: Medvigy, D., S. C. Wofsy, J. W. Munger, D. Y. Hollinger, and P. R. Moorcroft (2009), Mechanistic scaling of ecosystem function and dynamics in space and time: Ecosystem Demography model version 2, *J. Geophys. Res.*, *114*, G01002, doi:10.1029/2008JG000812.

1. Introduction

[2] Terrestrial biosphere models developed over the past two decades have been an important vehicle for inference about how terrestrial ecosystems will respond to changes in climate and atmospheric CO_2 levels, and how resulting changes in ecosystem structure, composition, and function will feed back and affect the atmosphere. Because the biological processes governing terrestrial ecosystem dynamics operate on a wide range of spatial and temporal scales, individual measurement programs only yield information on a subset of the processes governing the dynamics of vegetation change and belowground decomposition. For example, eddy-flux towers measure net carbon uptake by terrestrial ecosystems on timescales ranging from hours to decades, but only at spatial scales of 1 km^2 or smaller [*Wofsy et al.*, 1993; *Baldocchi et al.*, 1996]; satellite-derived estimates of leaf phenology provide information on seasonal-to-interannual changes in vegetation, but only with regard to foliar cover; and forest inventories provide information on aboveground structural components at spatial scales ranging from individual trees to the continent, but typically only at annual-decadal scales [*Frayer and Furnival*, 1999; *Penner et al.*, 1997].

[3] The conventional approach to evaluating terrestrial biosphere models has been to assess their ability to reproduce regional or global patterns of 'potential' (i.e., inferred pre-human settlement) vegetation, and seasonal-interannual patterns of CO_2 concentrations measured at remote atmospheric flask monitoring stations. Results from 'off-line' model intercomparisons indicate that most terrestrial biosphere models are able to replicate inferred patterns of potential vegetation and seasonal patterns of changes in regional atmospheric

[1]School of Engineering and Applied Sciences, Harvard University, Cambridge, Massachusetts, USA.
[2]Now at Department of Civil and Environmental Engineering, Duke University, Durham, North Carolina, USA.
[3]School of Engineering and Applied Sciences and Department of Earth and Planetary Sciences, Harvard University, Cambridge, Massachusetts, USA.
[4]Northern Research Station, USDA Forest Service, Durham, New Hampshire, USA.
[5]Department of Organismic and Evolutionary Biology, Harvard University, Cambridge, Massachusetts, USA.

0148-0227/09/2008JG000812$09.00

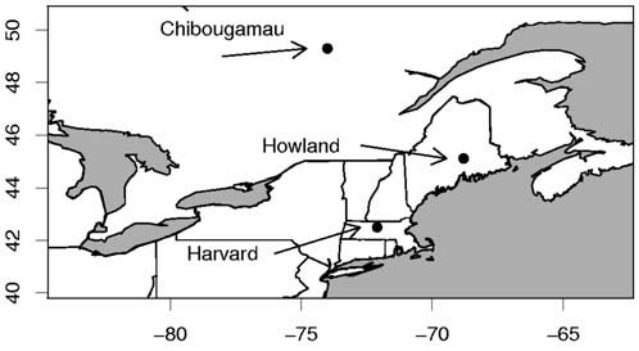

Figure 1. Relative locations of Harvard Forest, Howland Forest, and Chibougamou, Quebec. Harvard Forest, where ED2 was optimized, is 390 km from Howland Forest and 770 km from Chibougamou.

CO_2. However, the models diverge significantly in their predictions of ecosystem composition, structure, and functioning under novel climates [*Melillo et al.*, 1995; *Cramer et al.*, 2001; *Friedlingstein et al.*, 2006]. In coupled simulations, these differences feed back onto the atmosphere, resulting in different climate trajectories. As a result, terrestrial ecosystem responses to changes in climate and CO_2 are one of the largest sources of uncertainty for predicting future changes in climate [*Dufresne et al.*, 2002; *Denman et al.*, 2007]. The reasons for these differences in predicted ecosystem response include: differences in the sensitivity of plants to CO_2 and N fertilization, uncertainty in ecosystem responses to moisture stress, differential responses of soil mineralization to changing temperatures, and differences in the treatments of spatial heterogeneity in ecosystem composition and structure.

[4] The above considerations imply that the conventional approach to evaluating terrestrial biosphere models is insufficient for developing robust predictions of long-term ecosystem change [*Moorcroft*, 2006]. Accordingly, there have been a number of recent efforts that have used ecosystem measurements to constrain the behavior of terrestrial biosphere models [*Raupach et al.*, 2005; *Trudinger et al.*, 2007]. Such techniques can be used to optimize model parameters and obtain information on parameter uncertainties and covariances. In particular, several studies have used assimilation techniques to incorporate flux tower measurements into models. *Wang et al.* [2001] used three weeks of eddy-flux measurements to estimate photosynthesis and stomatal conductance parameters of a simplified terrestrial biosphere model designed to predict seasonal-to-interannual carbon fluxes, but found that site-specific model parameters were required to match the observations; similarly, *Reichstein et al.* [2003] optimized an ecosystem model using CO_2 and H_2O fluxes from Mediterranean ecosystems, but also found that site- and season-dependent model parameters were required. It appears that simplified biosphere and ecosystem models may not be able to make reliable predictions for locations and time periods other than those used in the model fitting.

[5] A further major challenge was illustrated by *Braswell et al.* [2005], who sought to constrain a terrestrial biosphere model against ten years of Harvard Forest CO_2 flux measurements. Unlike other commonly used models [*Wang et al.*, 2001; *Reichstein et al.*, 2003; *Knorr and Kattge*, 2005; *Wang et al.*, 2007], their model explicitly tracked changes in aboveground and soil carbon pools, thus potentially capturing the dynamics of longer-term processes such as forest succession that influence carbon fluxes over decadal to centennial scales. While their predictions for daily to annual net carbon fluxes improved significantly, their optimized model gave rise to unrealistic long-term carbon dynamics with excessive rates of carbon sequestration in vegetation and excessive decomposition of soil carbon stocks.

[6] A characteristic feature of the models used in the above studies is their use of a 'canopy as big-leaf' approximation, in which ecosystem response at large scales is represented as that of a single plant experiencing spatially averaged resource conditions. Ecological research over the past three decades [*Botkin et al.*, 1972; *Shugart and West*, 1977; *Huston et al.*, 1988; *Urban*, 1990; *Huston*, 1992; *Pacala et al.*, 1996] has shown, however, that because of the combination of spatially localized resource competition within plant canopies and the nonlinear relationships between plant resource availability and plant growth, mortality, and recruitment rates, knowing the dynamics of an average plant sitting in an average environment does not provide sufficient information for predicting the long-term dynamics of a heterogeneous plant canopy [*Levin et al.*, 1997]. These considerations call into question the capability of models using a 'big-leaf' approximation to reliably simulate long-term vegetation change.

[7] In this analysis, we adopt a different approach, using a combination of eddy-flux measurements, satellite-derived phenology observations, and forest inventory data obtained over a two-year period at Harvard Forest (42.5°N, 72.1°W) to constrain the dynamics of a structured terrestrial biosphere model, the Ecosystem Demography model version 2 (ED2) [*Medvigy*, 2006]. Instead of the conventional 'big-leaf' approximation, ED2 uses a system of partial differential equations to approximate the behavior of a spatially distributed ensemble of individual plants [*Hurtt et al.*, 1998; *Moorcroft et al.*, 2001; *Moorcroft*, 2003]. The equations and parameter values of ED2 thus incorporate the nonlinear impacts of fine-scale horizontal and vertical heterogeneity in ecosystem structure on both the plant-level carbon and water fluxes that underlie the canopy-scale exchange of CO_2 and H_2O with the atmosphere and the plant-level growth and mortality dynamics that underlie the long-term vegetation dynamics of the ecosystem.

[8] In this initial study we focus exclusively on ED2's representation of temperate ecosystems. In this context, we evaluate the constrained ED2 model's ability to scale correctly in time and space, comparing the model's predictions to measurements of seasonal-to-decadal scale vegetation and carbon dynamics at Harvard forest, seasonal-to-interannual carbon dynamics at Howland Forest and Chibougamou (Figure 1), and decadal vegetation dynamics in the northeastern United States and Quebec. The results show how the explicit representation of fine-scale heterogeneity in canopy structure enables ED2 to accurately capture regional-scale variation in carbon fluxes and vegetation dynamics across timescales of hours to decades.

2. Model Description

[9] The land surface in ED2 is subdivided into a series of grid cells that experience meteorological forcing from either

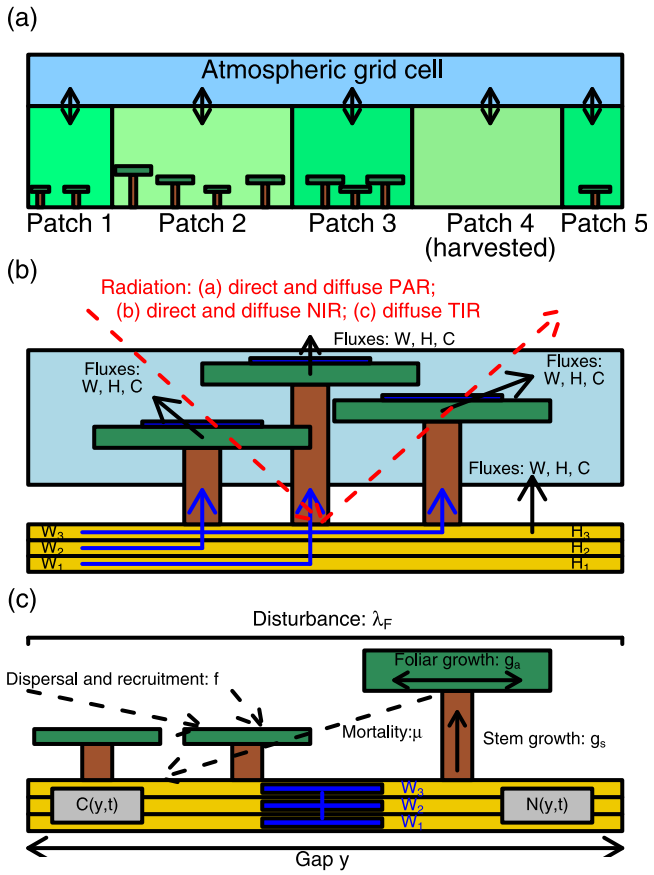

Figure 2. ED2 model structure and processes: (a) Each grid cell is subdivided into a series of tiles. The relative area of each tile is determined by the proportion of canopy-gap sized areas within the grid cell having a similar canopy structure as a result of a common disturbance history. (b) ED2 computes the multilayer canopy fluxes of water (W), internal energy (H) and carbon (C) within each subgrid scale tile. (c) Summary of the long-term vegetation dynamics within each tile arising from the integration of short-term fluxes shown in Figure 2b. Plant structural and living tissues grow at rates g_s and g_a, respectively; canopy mortality occurs at rate μ, and recruitment occurs at rate f. Recruits are dispersed within and between gaps. Rates g_s, g_a, μ and f vary as a function of the type x, size z and resource environment r of the plants. Disturbances occur at rate λ_F calculated by the disturbance submodel (canopy gap formation, fire and land use change). Hydrological and decomposition submodels track the accompanying dynamics of water (W), carbon (C) and nitrogen (N) within each tile.

corresponding gridded data sets of near-surface conditions or interactively from a coupled prognostic atmospheric model [*Medvigy*, 2006]. The grid cells can vary in size, ranging from the order of $\sim 10^2$ km when performing global scale simulations to the order of $\sim 10^{-1}$ km when performing regional or local scale simulations. Even at these smaller spatial scales, ecosystems are extremely heterogeneous. Some of this heterogeneity is abiotic, arising from fine-scale variation in physical attributes such as soil characteristics and topography. However, significant biotic heterogeneity also develops even in physically homogeneous environments as a result of natural disturbance processes such as wind-throw and fire, and anthropogenic disturbances such as forest harvesting, land clearing, and land-abandonment.

[10] Like its predecessor ED, ED2 captures subgrid scale biotic heterogeneity arising from disturbance events using a system of size- and age-structured partial differential equations (PDEs) that closely approximate the ensemble mean behavior of a corresponding individual-based stochastic gap model [*Moorcroft et al.*, 2001]. These PDEs are solved using the method of characteristics, subdividing each grid cell into a series of dynamic horizontal tiles, representing locations within the grid cell that have experienced a similar disturbance history, and with an explicit dynamic vertical canopy structure within each tile (Figure 2). Note that abiotic subgrid scale heterogeneity is not currently represented in the model.

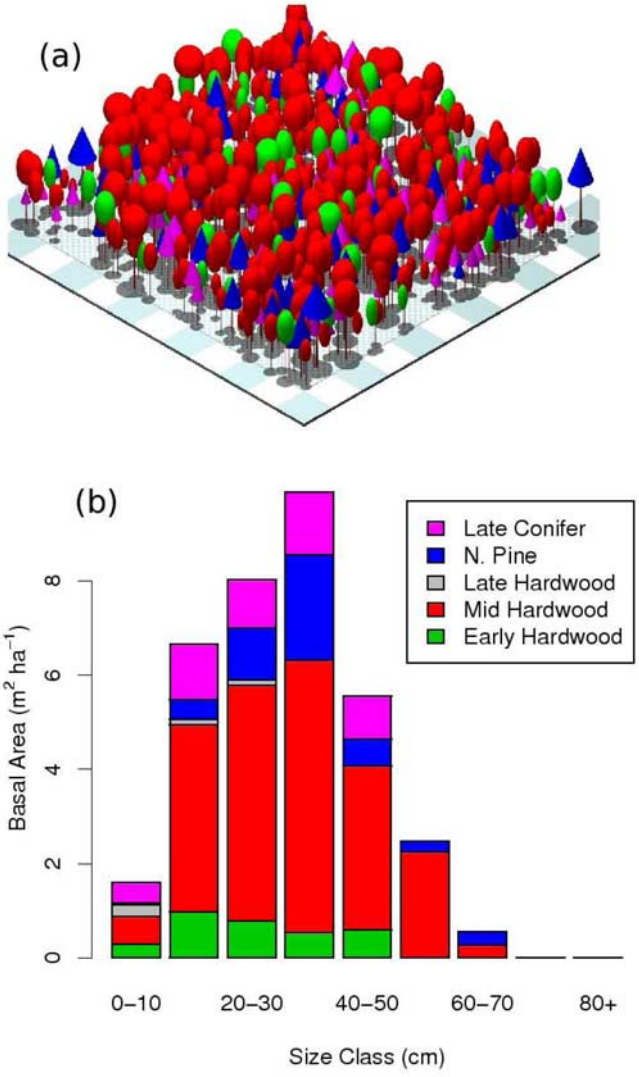

Figure 3. (a) Visualization of the ecosystem composition in the Harvard Forest flux tower footprint. Midsuccessional hardwoods (red) dominate, but the footprint also contains early successional hardwoods (green), pines (blue), late successional conifers (magenta) and late successional hardwoods (gray). (b) Distribution of basal area of the different plant functional types across tree diameter classes.

Table 1. Summary of Plant Functional Types

Plant Functional Types	Species
Early successional hardwood	*Betula Papyrifera, Betula Populifolia, Betula Lenta, Prunus spp.*
Midsuccessional hardwood	*Quercus rubra, Quercus velutina, Acer rubrum, Fraxinus Americana, Sorbus microcarpa Pursh.*
Late successional hardwood	*Acer saccharum, Fagus spp., Betula alleghaniensis*
Northern pine	*Pinus resinosa, Pinus strobus*
Late successional conifer	*Thuja occidentalis, Picea rubens, Picea glauca, Tsuga canadensis, Abies balsamea*

ED2 differs from the original ED model formulation by incorporating the biophysical components necessary for predicting short-term fluxes of CO_2, moisture, and energy. As a result, ED2 accounts for nonlinear interactions between short-term and long-term processes, and can be either forced directly with fast timescale meteorological data, or interactively coupled with atmospheric models. Further details on the ED2 model be found in *Medvigy* [2006] and in the appendices of this paper.

3. Analysis

[11] Before optimizing the model, we performed an initial 11-year simulation from 1993 through 2003. Our parameterization was taken directly from the North American parameterization of ED [*Albani et al.*, 2006], whose parameterizations and parameter values are based on those found in a number of other biosphere models [*Foley et al.*, 1996; *Haxeltine and Prentice*, 1996; *Friend et al.*, 1997]. This initial model thus reflected our prior quantitative understanding of vegetation dynamics within the region.

[12] The model was forced with measurements of short and longwave radiation, air temperature, precipitation, relative humidity, wind speed, and pressure, which have been taken at Harvard Forest since October 1991, except for longwave radiation, which has only been measured since 2001. Occasional gaps in the climatological data caused by power failures, recalibration periods, and extreme precipitation events were filled with data from the NCEP reanalysis data set [*Kalnay et al.*, 1996]. The NCEP reanalysis data set was also used to prescribe the initial conditions for the soil moisture and soil temperature profile. The depth of the mineral soil and the soil textural class were prescribed from the 1 km^2 STATSGO data set [*Miller and White*, 1998].

[13] Ecosystem composition was initialized from a forest inventory conducted in the footprint of the Harvard Forest eddy-flux tower. The forest inventory included censuses of all trees larger than 10 cm diameter at breast height (DBH) in forty plots of 10 m radius conducted in 1992, 1997, and annually thereafter. One additional census of trees between 1 and 10 cm DBH was conducted in 2005. The composition determined from the 1992 census and 2005 understory is illustrated in Figure 3. As can be seen in the figure, hardwoods comprise about ~75% of the basal area, with the dominant species being northern red oak (*Quercus Rubra* L.) and red maple (*Acer Rubrum* L.).

[14] Because the canopy-gap scale distribution of times since last disturbance within the tower footprint is not known, horizontal heterogeneity in canopy composition was represented by grouping the inventoried plots into series of distinct subgrid scale tiles based on their similarity in vertical structure and composition. The compositional profile within each tile was represented explicitly, assigning all trees to their corresponding plant functional type (PFT) (Table 1).

[15] Results from this initial simulation, shown in Table 2, indicate large RMS errors in the model's predictions of carbon fluxes and tree growth and mortality. For example, the RMS error of the annual net ecosystem productivity or NEP (3.1 tC ha^{-1} a^{-1}) exceeds the observed mean NEP of 2.4 tC ha^{-1} a^{-1}. Moreover, the model predicts an average growth rate of 1.22 m^2 ha^{-1} a^{-1}, approximately four times higher than the observed mean rate of 0.32 m^2 ha^{-1} a^{-1}. Predicted mortality rates also have a large RMS error (1.5 m^2 ha^{-1} a^{-1}), mainly because of overestimation during the first few years of the simulation.

3.1. Model Reformulation

[16] The above simulation motivated three adjustments to the model formulation prior to optimization. First, the leaf area index (LAI) of the tower footprint calculated using the initial model's allometric parameterization was 6.5, substantially higher than the LAI of 4 measured in the tower footprint. This discrepancy was corrected by modifying the leaf area-DBH relationships for early and midsuccessional hardwoods (Table 3) to match the empirical allometry estimates of *Ter-Mikaelian and Korzukhin* [1997] and *Villar and Merino* [2001]. These yield an LAI of 4.05 for the tower footprint, closely matching the observed LAI.

[17] Second, the overprediction of NEP was in part due to a spuriously early start to the growing season (Figure 4a). This

Table 2. RMS Errors of ED2 Simulations of Harvard Forest

Data Set	Units	RMS Error: Initial Model	RMS Error: Optimized Model, HET	RMS Error: Optimized Model, AGG	RMS Error: Optimized Model, HOM
Annual NEP	tC ha^{-1} a^{-1}	3.1	1.0	1.1	0.7
Monthly NEP	tC ha^{-1} $month^{-1}$	0.67	0.29	0.26	0.25
Daytime NEP	tC ha^{-1} $month^{-1}$	1.0	0.46	0.46	0.73
Nighttime NEP	tC ha^{-1} $month^{-1}$	1.1	0.26	0.18	0.44
Total growth	m^2 ha^{-1} a^{-1}	0.86	0.09	0.13	0.10
Hardwood growth	m^2 ha^{-1} a^{-1}	0.74	0.08	0.14	-
Conifer growth	m^2 ha^{-1} a^{-1}	0.13	0.03	0.04	-
Total mortality	m^2 ha^{-1} a^{-1}	1.5	0.35	0.37	0.16
Hardwood mortality	m^2 ha^{-1} a^{-1}	1.3	0.13	0.13	-
Conifer mortality	m^2 ha^{-1} a^{-1}	0.27	0.29	0.34	-

Table 3. Eco-Physiological, Life-History, and Allometric Parameters for the Plant Functional Types[a]

Property	Early Successional Hardwoods	Midsuccessional Hardwoods	Late Successional Hardwoods	Northern Pines	Late Successional Conifers	C_3 Grasses and Forbs
Leaf habit	CD	CD	CD	E	E	DD
SLA (m^2 (kg C)$^{-1}$)	40 (30)	30 (24)	60	6	10	22
Density independent mortality rate (a^{-1})	0.006	0.004	0.004	0.003	0.001	0.07
Global dispersal (fraction)	1	0.33	0.07	0.77	0.001	1
V_{m0} (μmol m^{-2} s^{-1})	18.3 (20.1)	15.6 (17.2)	6.3 (6.9)	15.6 (11.4)	6.3 (4.6)	18.3
l_1 (kg C)	0.0047 (0.013)	0.024 (0.048)	0.017	0.024	0.045	0.08
l_2	2.25 (1.75)	1.86 (1.46)	1.73	1.9	1.68	1.0
h_1 (m)	22.68	25.2	23.4	27.1	22.8	0.48
h_2 (cm^{-1})	-0.065	−0.05	−0.054	−0.039	−0.044	−0.75
s_1 (kg C)	0.026	0.16	0.23	0.15	0.16	1×10^{-5}
s_2	2.96	2.46	2.25	2.24	2.15	1

[a]The initial and optimized model used the same values except for the parameters SLA, V_{m0}, l_1 and l_2; for these, optimized model values are in parentheses. The leaf habits include CD, cold deciduous; DD, drought deciduous; E, evergreen.

occurred because the predictive, climate-driven phenology model [*Botta et al.*, 2000] predicts hardwood leaf-flush in early May, while ground-based measurements of spring leaf elongation indicate that hardwoods do not fully flush until mid-June. This mis-match was eliminated by replacing the *Botta et al.* [2000] phenology model with a prescribed phenology model, which uses MODIS-derived estimates for the beginning and end of spring leaf-flush and fall leaf-drop [*Zhang et al.*, 2003] to parameterize two logistic functions describing the pattern of fractional leaf-out during the year (Appendix B). The predictions of this regional prescribed phenology model (Figure 4a) closely match ground-based observations of leaf phenological status conducted at Harvard Forest since 1992 (data available at http://harvardforest.fas.harvard.edu/data/p00/hf003/hf003.html), with the additional advantage of yielding empirically constrained estimates of phenological status for locations where ground-based measurements are not available. In addition, the physiological submodel was modified to capture the decline in leaf photosynthetic capacity arising from leaf aging [*Wilson et al.*, 2000] that precedes the decline in leaf color at the end of the growing season (equation (B4)).

[18] Third, the summertime plant respiration predicted by the initial model formulation was nearly equal to the observed nighttime total ecosystem (plant plus heterotrophic) respiration (Figure 4b). This high summertime plant respiration is primarily the result of high modeled levels of growth respiration by hardwoods during the growing season. Consistent with earlier terrestrial biosphere model formulations [*Foley et al.*, 1996; *Friend et al.*, 1997; *Haxeltine and Prentice*, 1996; *Knorr*, 2000], the initial model formulation assumes that one third of the carbon assimilated by the canopy is lost instantaneously as growth respiration. This formulation derives primarily from measurements of herbaceous plants [*Amthor*, 1984, 2000; *van Iersel*, 2003], while measurements on trees are much rarer (though see *Paembonan et al.* [1992]).

[19] As seen in Figure 4b, this formulation is inconsistent with canopy-scale measurements of carbon fluxes: during the summer the modeled nighttime plant respiration alone is larger in magnitude than the observed nighttime NEP, which includes both plant and heterotrophic respiration. We addressed this problem by reformulating the hardwood growth submodel, replacing hardwood growth respiration with a maintenance loss term on the hardwood stored carbon pool

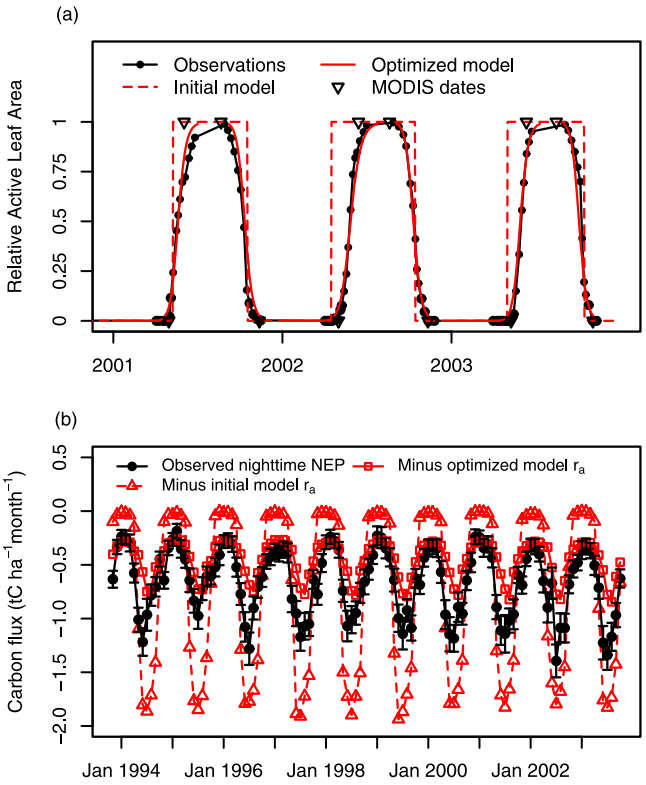

Figure 4. (a) Leaf phenology at Harvard Forest. The on-the-ground observations of fractional leaf elongation (spring) and leaf coloration (fall) are in black and the dashed red line is the original climate-based phenology model of *Botta et al.* [2000], in which the timing of leaf onset and offset occurs instantaneously at dates determined by climatological conditions. Black triangles indicate the MODIS dates [*Zhang et al.*, 2003] used in the prescribed phenology model in which leaf onset and offset are determined by a continuous function (red line). The optimized model yields significant improvement at Harvard Forest and is easily generalizable to other sites where on-the-ground phenology data are unavailable. (b) Observed nighttime NEP and model predictions of plant respiration (r_a). In the initial model formulation, summertime r_a alone is larger in magnitude than the observed NEP. In contrast, in the modified, optimized plant respiration formulation (equation (C10)), summertime r_a has a smaller magnitude than the observed NEP.

Table 4. Summary of Data Sets Used to Constrain ED2

Source	Metric	Aggregation	Number of Observations
Tower			
	Net ecosystem productivity (NEP; tC m^{-2} a^{-1})	Annual	2
		Monthly	24
		Hourly, daytime	6753
		Hourly, nighttime	6783
	Evapotranspiration (mm h^{-1})	Hourly	9949
Forest Inventory			
	Growth (m^2 ha^{-1})	hardwood	6
		coniferous	6
		combined	2
	Mortality (m^2 ha^{-1})	hardwood	6
		coniferous	6
		combined	2

(Appendix C). This results in a more even distribution of hardwood respiration throughout the year.

3.2. Model Optimization

3.2.1. Model Configurations

[20] We carried out three model optimizations, differing in their representations of heterogeneity in vegetation composition and structure. In our standard optimization ('HET'), horizontal heterogeneity was represented in the model by using the individual observation plots to initialize individual subgrid-scale tiles in ED2. In contrast, in our aggregated optimization ('AGG'), all trees in the observed plots were averaged together into a single ED2 tile. Note that this averaging was applied to horizontal structure only, with the result that both HET and AGG contained vertically heterogeneous canopies consisting of different plant functional types. Our third optimization ('HOM') also grouped all trees into a single ED2 tile; however, unlike AGG, all trees were here assigned to the same plant functional type. Thus, in HOM the vegetation properties are homogeneous both in the horizontal and in the vertical, and is most similar to models using a typical 'ecosystem as big-leaf' approximation.

3.2.2. Data Sets and Parameters

[21] We used ecosystem measurements from a two-year period, November 1994-October 1996, to estimate 14 model parameters. This period was selected because it has a relatively complete flux-tower time-series that includes both a hot and dry summer (1995) and a cool and damp summer (1996). Simulations were initialized in January 1993 to minimize any transient dynamics arising from the initial soil moisture and temperature conditions.

[22] Maximum likelihood was used to estimate model parameters, uncertainties, and covariances from observational data sets (Table 4): (i) annual net ecosystem production (NEP); (ii) monthly NEP; (iii) hourly daytime NEP; (iv) hourly nighttime NEP; (v) hourly evapotranspiration (ET); (vi) basal area increment (BAI) of all trees in the tower footprint; (vii) mortality of all trees in the tower footprint; (viii) BAI of hardwood and coniferous trees in three DBH size classes (10–20 cm, 20–30 cm and over 30 cm); (ix) mortality of hardwood and coniferous trees in three DBH size classes (10–20 cm, 20–30 cm and over 30 cm). All data sets (i)–(ix) were used for the HET and AGG optimizations, but the HOM optimization used only data sets (i)–(vii) because it did not distinguish between plant functional types. It has previously been shown that this approach of using several data sets, including both flux tower and forest inventory measurements, allows different model components to be simultaneously optimized [*Williams et al.*, 2005]. Furthermore, disaggregating NEP into daytime (data set iii) and nighttime (data set iv) components can be viewed as a way of distinguishing respiration from the difference of photosynthesis minus respiration, in effect allowing the model's predictions of both respiration and photosynthesis components of the ecosystem's net carbon fluxes to be constrained [*Mahadevan et al.*, 2008].

[23] Ten vegetation parameters, common to many dynamic vegetation models, were selected for the optimization of HET and AGG (Table 5) on the basis that (i) previous estimates have come from studies focusing on different spatial scales,

Table 5. Summary of Optimized Parameters[a]

Parameter	Symbol	Initial Value	Optimized Value and 2σ Uncertainty, HET	Optimized Value and 2σ Uncertainty, AGG	Optimized Value and 2σ Uncertainty, HOM	Reference (Equation No.)
Stomatal Slope	M	8	6.4 (1.3)	6 (6)	>0	equation (B15)
Hardwood V_{m0} multiplier	$V_{mult,hw}$	1	1.1 (0.08)	0.71 (0.20)	0.4 (0.1)	equation (B4)
Conifer V_{m0} multiplier	$V_{mult,co}$	1	0.73 (0.10)	0.76 (0.38)	-	equation (B4)
Photosynthesis temperature threshold (°C)	$T_{V,lo}$	5	4.7 (2.3)	5 (7)	14 (<18)	equation (B4)
Fine root turnover rate (a^{-1})	α_{root}	0.333	5.1 (0.5)	2.0 (0.9)	0.01 (1.3)	equation (C6)
Allocation to fine roots relative to leaves, hardwoods	q_{hw}	1	1.1 (0.2)	1.4 (1.3)	2.4 (5.5)	equation (C1)
Allocation to fine roots relative to leaves, conifers	q_{co}	1	0.35 (0.07)	0.8 (0.5)	-	equation (C1)
Water availability parameter (m^2 a^{-1} (kgC root)$^{-1}$)	K_W	160	150 (1200)	170 (92)	230 (>5)	equation (B22)
Conifer growth respiration fraction	$r_{g,co}$	0.333	0.45 (0.06)	0.35 (0.17)	-	equation (C4)
Hardwood growth respiration fraction	$r_{g,hw}$	0.333	-	-	-	equation (C4)
Hardwood storage respiration rate (a^{-1})	$\alpha_{storage,hw}$	-	0.62 (0.08)	0.49 (0.16)	0.5 (0.3)	equation (C10)
Optimal temperature (°C)	T_{opt}	35	-	-	-	equation (D1)
Temperature convexity parameter	t_1	0.19	-	-	-	equation (D4)
Temperature convexity parameter	t_2	1.8	-	-	-	equation (D4)
Optimal soil moisture (m^3 m^{-3})	W_{opt}	0.6	0.89 (0.04)	0.88 (0.13)	0.5 (0.5)	equation (D3)
Soil moisture convexity parameter	w_1	5.0	5.1 (1.8)	6 (10)	13 (>0)	equation (D3)
Soil moisture convexity parameter	w_2	5.6	4.5 (5.8)	6 (39)	7 (>0)	equation (D3)
Temperature Q_{10}	Q_{10}	-	2.13 (0.09)	1.93 (0.39)	3.3 (>2.2)	equation (D5)

[a]Note that the initial model included $r_{g,hw}$, T_{opt}, t_1 and t_2 but not $\alpha_{storage,hw}$ or Q_{10}; the optimized models included $\alpha_{storage,hw}$ and Q_{10} but not $r_{g,hw}$, T_{opt}, t_1 or t_2. Optimized parameter values are the maximum likelihood estimates (see section 3.2). For the HET optimization, the likelihood function was highly asymmetric with respect to K_W; its one-sided uncertainties were +1200, −28. The HET optimization had much smaller uncertainty intervals than the AGG or HOM optimizations.

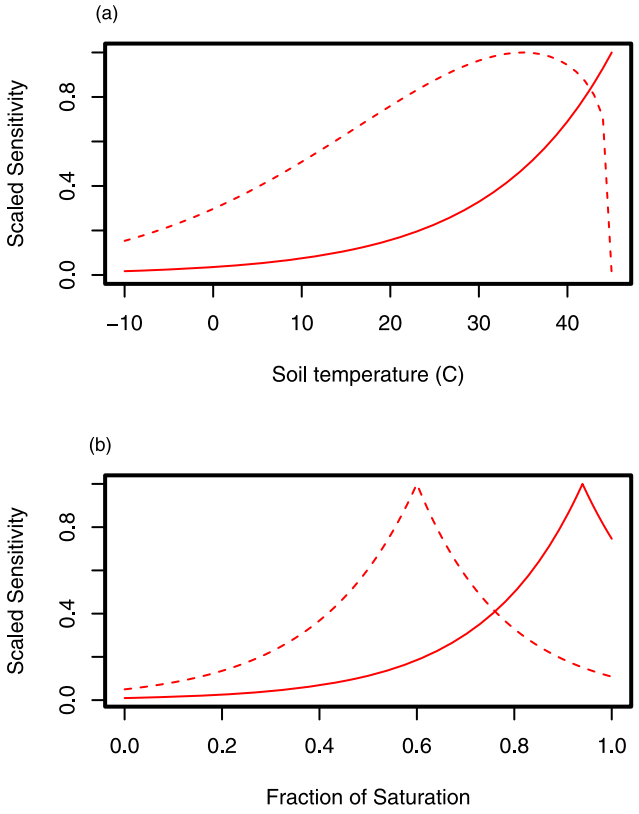

Figure 5. Dependence of heterotrophic respiration on (a) temperature and (b) moisture. The dashed red curves represent the initial 6-parameter model and the solid red curves represent the optimized 4-parameter model (see Appendix D).

and thus carrying the potential for biases [*Rastetter et al.*, 1992] and/or (ii) despite being commonly used in models, they remain poorly constrained by direct measurements. Three of these parameters exert a direct control on the fast timescale fluxes of CO_2 and H_2O: M, the slope of the stomatal conductance-photosynthesis relationship (equation (B15)),

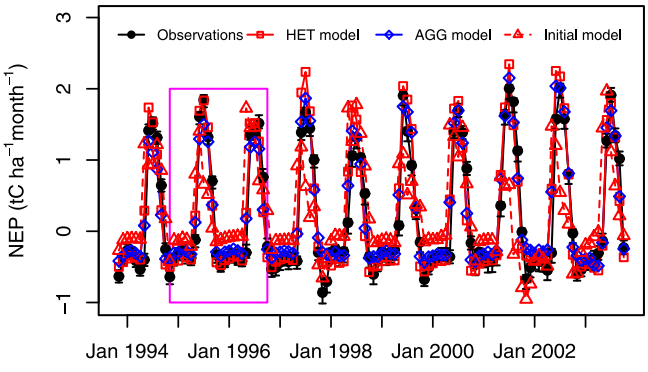

Figure 6. Predicted and observed patterns of monthly Net Ecosystem Productivity (NEP; tC ha^{-1} $month^{-1}$) at the Harvard flux tower. The black line represents the observations, the solid red line indicates the predictions from the HET run, the blue line indicates the predictions from the AGG run, and the dashed red line indicates the predictions from the initial model. The magenta box indicates the observations used to optimize the model.

and $V_{mult,hw}$ and $V_{mult,co}$—multipliers used to scale the intrinsic photosynthetic capacities (V_{m0}) of the deciduous and coniferous plant functional types (equation (B3) and Table 3). Three parameters affecting plant efficiency, conifer growth respiration, r_g (equation (C4)),the turnover rate of stored carbohydrates in hardwoods, $\alpha_{storage}$ (equation (C10)), and the turnover rate of fine roots, α_{root} (equation (C6)), were also optimized. The remaining optimized parameters that directly impacted the vegetation included the temperature below which photosynthesis begins to rapidly decline, $T_{V,lo}$ (equation (B3)), the allocation of carbon to fine roots relative to leaves in hardwoods and conifers, q_{hw} and q_{co}, respectively (equation (C1)), and K_W, which governs water availability per unit root biomass (equations (B20) and (B21)). Because the HOM optimization did not distinguish plant functional types, it excluded the three parameters $V_{mult,co}$, r_g, and q_{co}.

[24] All of the parameters controlling the temperature and moisture dependencies of decomposition were optimized (Appendix D). In addition to the coefficients of the 6-parameter temperature and moisture dependency function of the initial model formulation (equations (D3) and (D4)), we also estimated the coefficients of a simpler 4-parameter

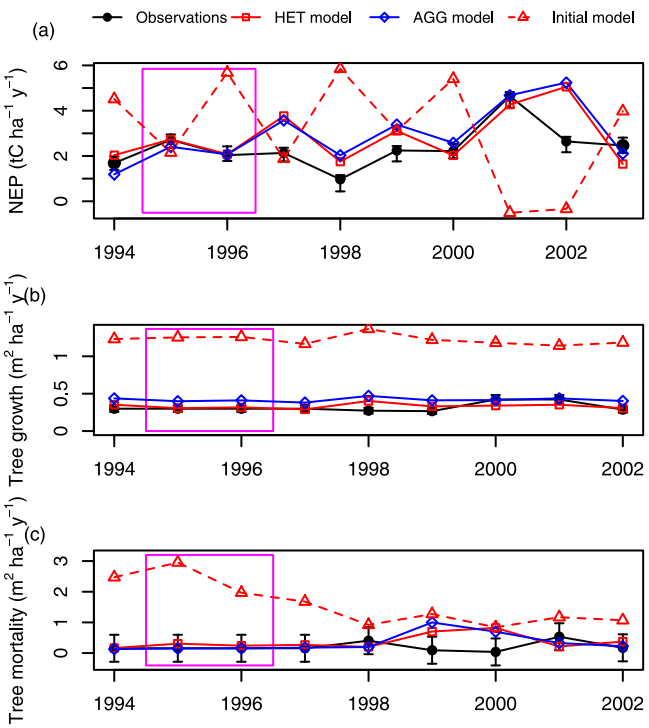

Figure 7. Predicted and observed patterns of Net Ecosystem Productivity (NEP) and rates of tree growth and mortality at Harvard Forest. (a) Annual NEP in tC ha^{-1} a^{-1}. The black lines indicate the flux-tower measurements, the solid red lines indicate the predictions of the HET model, the blue lines indicate the predictions of the AGG model, and the dashed red lines indicate the predictions from the initial model. Error bars indicate the 2σ error estimates for the observations and the magenta boxes indicate the two years of observations used to optimize the model. (b) Annual growth rates of trees within the flux tower footprint shown in units of basal area increment (m^2 ha^{-1} a^{-1}). (c) Annual rates of mortality shown in units of basal area loss (m^2 ha^{-1} a^{-1}).

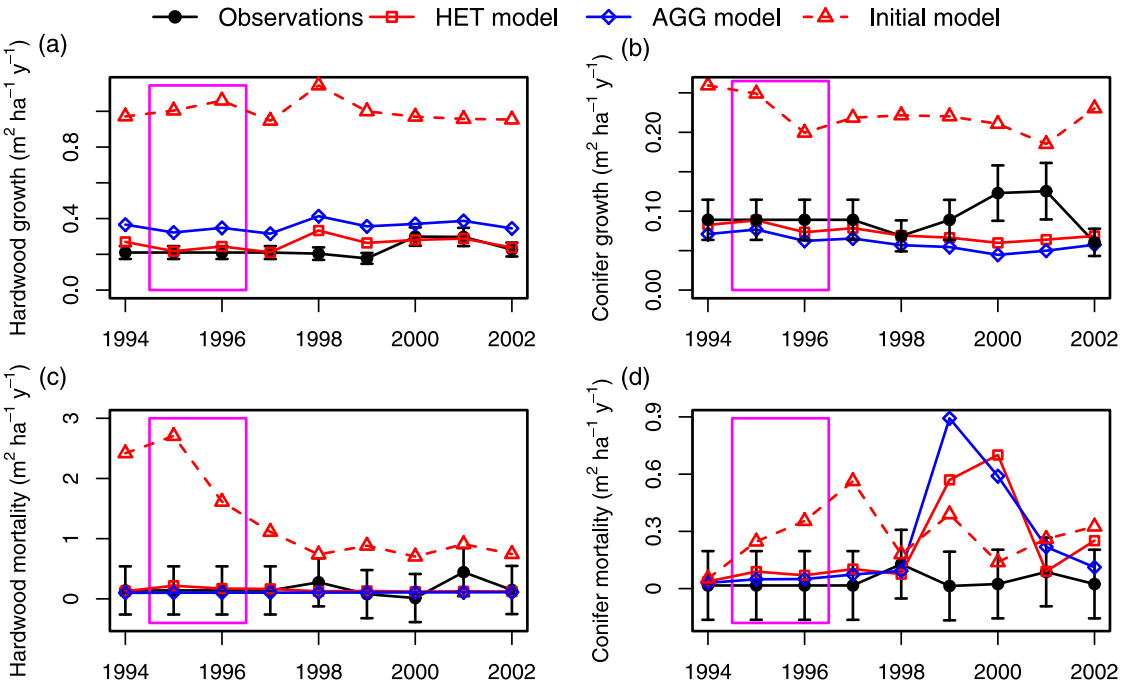

Figure 8. Annual basal area growth and mortality rates for hardwoods and conifers at Harvard Forest. The magenta box indicates the two years of observations used to optimize the model parameters. The black lines indicate the observations, the solid red lines indicate the predictions of the HET model, the blue lines indicate the predictions of the AGG model, and the dashed red lines indicate the predictions from the initial model. (a) Basal area increment (BAI) for hardwoods and (b) BAI for conifers. (c and d) Mortality for hardwoods and conifers, respectively. 2σ error bars are shown for the observations.

temperature and moisture dependency function (equations (D5) and (D3)).

3.2.3. Maximum Likelihood Method

[25] The method of maximum likelihood [*Edwards*, 1972] was used to determine the set of model parameters most supported by the data sets and their uncertainties. Model parameters were chosen so as to maximize the following log-likelihood function, S, given by:

$$S = \sum_{j=1}^{N_{datasets}} \left(\frac{1}{N_j} \sum_{i=1}^{N_j} s_{ij} \right). \quad (1)$$

where N_j is the number of observations in data set j and s_{ij} is contribution to the log-likelihood from element i of data set j.

[26] With the exception of the hourly flux measurements, all data sets were assumed to have normally distributed measurement errors. In this case,

$$s_{ij} = -\frac{1}{2} \left(\frac{x_{pred,ij} - x_{obs,ij}}{\sigma_{ij}} \right)^2. \quad (2)$$

Standard deviations of annual NEP were taken from *Urbanski et al.* [2007]. Each month was assumed to contribute an equal amount to the annual uncertainty. The standard deviation for the total BAI was taken from *Barford et al.* [2001], and the standard deviation for the mortality was set to be of the order of the measurement itself because ED2, as the first moment approximation to a stochastic gap model, predicts the expectation value of annual mortality, not the mortality experienced in individual years. The standard deviations associated with the differential BAI and mortality data sets were calculated such that each tree contributed equally to the standard deviation of its parent data set.

[27] Consistent with the analysis of *Hollinger and Richardson* [2005], the hourly measurements of daytime and nighttime NEP and evapotranspiration were assumed to have a double-exponential error distribution. In this case,

$$s_{ij} = \frac{\left| x_{pred,ij} - x_{obs,ij} \right|}{\sigma_{ij}}, \quad (3)$$

where σ_{ij} is the uncertainty in element i of data set j, $x_{obs,ij}$ is the measurement of element i in data set j and $x_{pred,i}$ is the prediction of element i in data set j. Following the formulations of *Hollinger and Richardson* [2005], the standard deviations for the hourly NEP and evapotranspiration were taken to be linear functions of the fluxes. Equation (1) was maximized using a numerical nonlinear simulated annealing maximization algorithm [*Press et al.*, 1992].

4. Results

4.1. Likelihood Scores and Parameter Estimates

4.1.1. Heterogeneous Vegetation Initialization

[28] In going from the initial model to the reformulated initial model (section 3.1), the log-likelihood score (equation (1)) improved from −192 to −178 and the Akaike Information Criterion (AIC) improved from 416 to 384. After parameter optimization, the model attained a log-likelihood score of −1.3 and an AIC of 31. To put the changes in log-likelihood into perspective, a significant change in goodness-of-fit would correspond to a change of only 2 log-likelihood units.

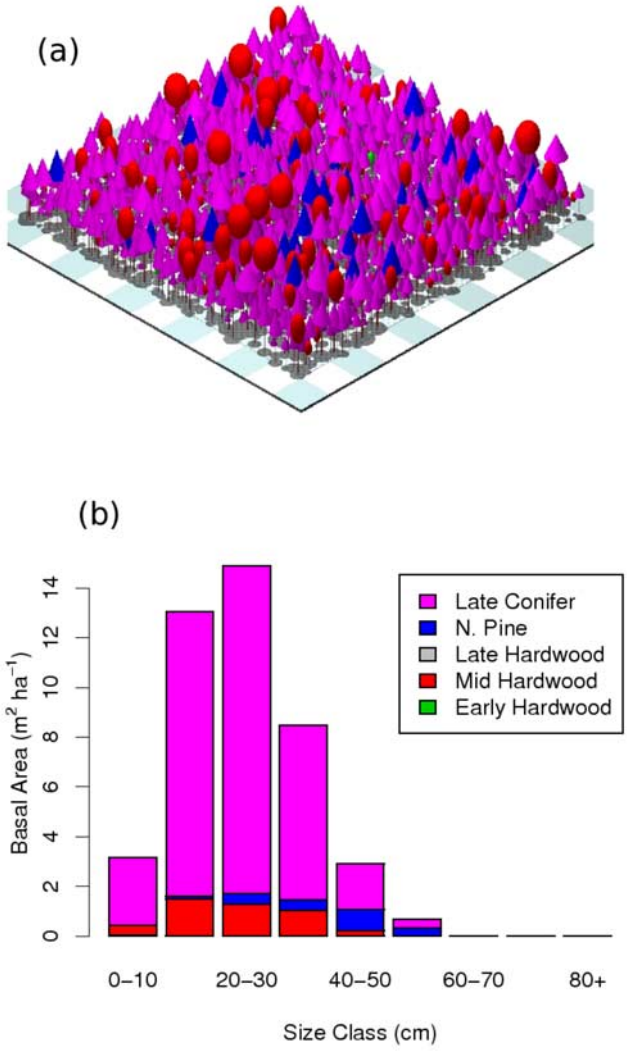

Figure 9. (a) Three-dimensional representation of the forest composition in the flux-tower footprint, and (b) forest composition in the forest inventory plots in Howland Forest flux-tower footprint broken down by PFT and size class. In contrast to Harvard, the forest composition at Howland is dominated by late successional conifers (magenta), but also contains midsuccessional hardwoods (red), pines (blue), and early successional hardwoods (green).

These results indicate that the parameter optimization caused most of the improvement in model performance, although the direct impact of model reformulation was not insignificant.

[29] The maximum likelihood estimates and confidence intervals for the optimized model parameters are given in Table 5. The optimization increases the maximum photosynthetic rate of hardwoods while decreasing that of conifers, slightly lowers the temperature threshold for photosynthesis, and reduces the slope of the relationship between stomatal conductance and photosynthesis (M).

[30] There are also changes in patterns of respiration, carbon allocation, and turnover. Conifer growth respiration increases from 0.33 to 0.45, while the turnover rate of stored carbon that replaced hardwood growth respiration in the optimized model is estimated to be 0.63 a^{-1}. The optimization also indicates different patterns of carbon allocation in hardwoods and conifers, with higher allocation to the belowground fine-root pools in hardwoods and lower belowground allocation in conifers, and an order of magnitude increase in the rate of fine-root turnover.

[31] Figure 5 shows the consequences of the decomposition-submodel parameter changes for the relative decomposition rates of the soil pool. As the figure indicates, the optimization reduces the temperature dependency of decomposition and significantly changes W_{opt}, the soil moisture level at which the decomposition rate is maximal, increasing it from 0.6 to 0.88. The 4-parameter decomposition formulation (Figure 5) gave just as good a fit to the respiration observations as an optimized version of the 6-parameter decomposition formulation (not shown).

[32] The 95% (2σ) confidence bounds indicate that most of the optimized vegetation parameters are well-constrained; excepting K_W and w_2, the average coefficient of variation is 18%. The lower confidence bound on K_W is also reasonably well-constrained, but the model's predictions are largely insensitive to it when it takes on values much greater than its optimum (Table 5). The model exhibits little sensitivity to w_2 because W_{opt} is close to one.

[33] The covariances between the optimized parameters are given in Appendix E. Because of several large covariances, no single parameter change is responsible for the improved results of the optimized model. However, a principal components analysis indicated that the likelihood function varied most strongly in the direction of changing net primary production (equal to photosynthesis minus plant respiration), which controlled rates of tree growth.

4.1.2. Aggregated and Homogeneous Vegetation Simulations

[34] Table 5 also lists the optimized parameters that resulted when the canopy was represented in a more aggregated manner. Except for two parameters, the parameters from the AGG optimization were consistent with those from the HET optimization. One difference was a smaller $V_{mult,hw}$, which leads to reduced hardwood photosynthesis, though this was balanced by a smaller α_{root}, which leads to reduced carbon costs for both hardwoods and conifers. In addition, the AGG estimate of q_{co} was over double the HET estimate. This difference increases conifer photosynthesis in the AGG run relative to the HET run by reducing water stress, but also increases carbon costs by increasing allocation to the rapidly turning-over pool of fine roots.

[35] The parameter uncertainties in the AGG optimization are, however, generally larger than in the HET optimization, illustrating the loss of information that accompanies homogenization of the plant canopy. This loss of information becomes even more acute with the HOM optimization, which, despite generally consistent parameter estimates, has substantially larger uncertainty intervals than the HET and AGG optimizations (Table 5). Only $V_{mult,hw}$ has an uncertainty less than 50% of its optimized value, while several parameters have unbounded uncertainty intervals.

4.2. Harvard Forest Carbon Fluxes and Vegetation Dynamics

[36] The two-year model optimization yielded greatly improved predictions of net ecosystem productivity (NEP) and vegetation dynamics over a full 10-year simulation (Table 2) using the HET vegetation initialization. The

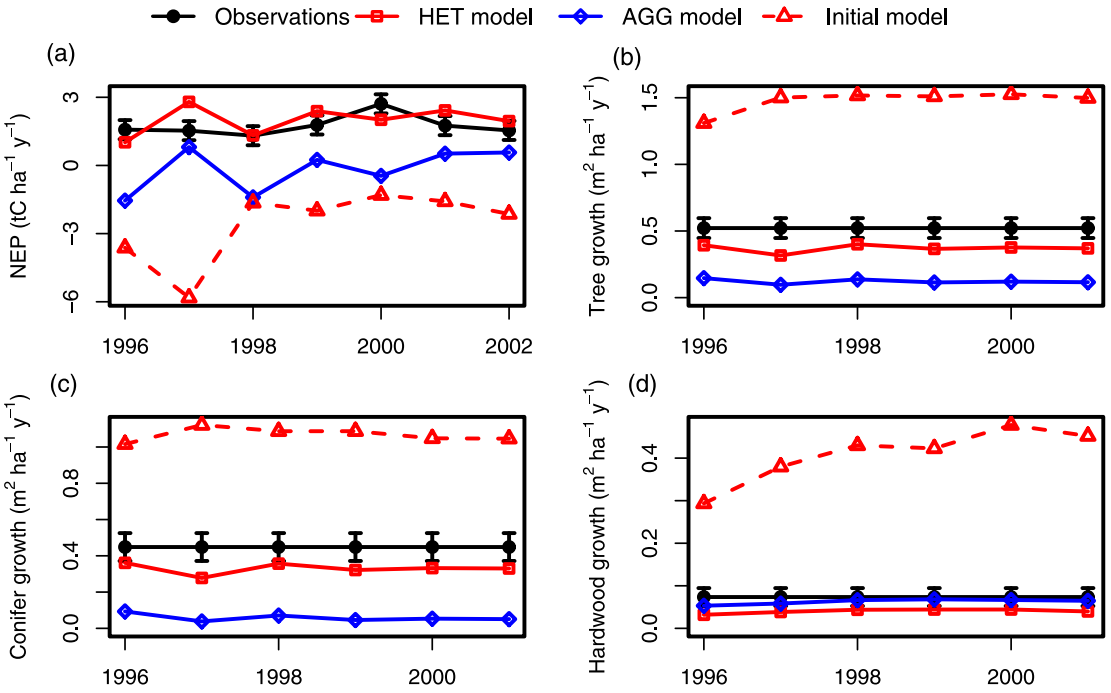

Figure 10. Patterns of annual net ecosystem productivity (NEP) and tree growth rates at Howland Forest for the period 1996–2002. The black lines represent the observations, the solid red lines indicate the predictions of the HET model, the blue lines indicate the predictions of the AGG model, and the dashed red lines indicate the predictions from the initial model. Vertical bars indicate the 2σ errors for the measurements. (a) Annual net ecosystem productivity (NEP; tC ha^{-1} a^{-1}). (b) Annual tree growth rates within the Howland flux tower footprint in units of basal area increment (m^2 ha^{-1} a^{-1}). While the AGG model strongly underpredicts NEP and tree growth, the HET model closely matches the observations. (c and d) Growth rates of conifers and hardwoods, respectively.

optimized model generally captures the observed seasonality (Figure 6), and yields realistic annual values for NEP (Figure 7a), although the model overpredicts NEP in the summers of 1997–1998. Rates of tree growth and mortality (Figures 7b and 7c) also correspond more closely with observations, except for overprediction of growth in 1998 and overprediction of mortality in 1999 and 2000.

[37] Because of its ability to represent biotic ecosystem heterogeneity, ED2 is by design able to distinguish between hardwood and conifer vegetation dynamics (Figure 8). In contrast to the initial model's systematic overpredictions hardwood and conifer growth, the optimized model yields significantly improved growth rates throughout the 10-year period (Table 2). Mortality rates of hardwoods also improve, with the optimized model's predictions lying within the data uncertainty estimates in all years. However, the RMS error in the optimized model's predicted conifer mortality rates becomes slightly higher than that of the initial model.

[38] The RMS errors from 10-year AGG and HOM runs (parameterized according to their respective optimizations; Table 5) are shown in Table 2. Model performance in these cases is also much improved over the initial model, and is on par with the HET simulation.

4.3. Regional Evaluation

4.3.1. Howland Forest

[39] We evaluated the HET and AGG ED2 model formulations developed at Harvard Forest against independent observations of carbon fluxes and vegetation dynamics at the Howland Forest (45.1°N, 68.8°W) eddy-flux tower site [*Hollinger et al.*, 2004]. Howland is located 390 km northeast of Harvard Forest (Figure 1), and has a markedly different forest composition, with conifers comprising approximately 90% of the basal area (Figure 9). For a detailed site description, see *Hollinger et al.* [1999]. As in the Harvard Forest simulations, ecosystem composition was directly initialized from the composition measured in 48 forest inventory plots located in the eddy-flux tower footprint; these plots remained distinct in the HET simulation, but were averaged horizontally in the AGG simulation. Soil carbon pools were set at their observed levels, the phenology was prescribed as described in section 3.1, and the observed meteorology was used to force the model. A 7-year period (1996–2002) was simulated, for which carbon flux and tree growth measurements were available (no mortality measurements were available at the Howland site). Note that no changes in model parameters were made prior to the simulations.

[40] In the HET run, ED2 realistically simulates annual NEP (Figure 10a), giving a bias of 0.25 tC ha^{-1} a^{-1}, corresponding to 14% of the observed mean NEP (1.74 tC ha^{-1} a^{-1}). Tree growth rates were systematically underestimated, with a bias of -0.15 m^2 ha^{-1} a^{-1}, corresponding to 29% of the observed mean. The AGG simulation compared less favorably to the observations (Figure 10). Annual NEP was systematically underpredicted (a bias of -2.1 tC ha^{-1} a^{-1} or -120%), as were rates of tree growth (bias of -0.40 m^2 ha^{-1} a^{-1} or -77%).

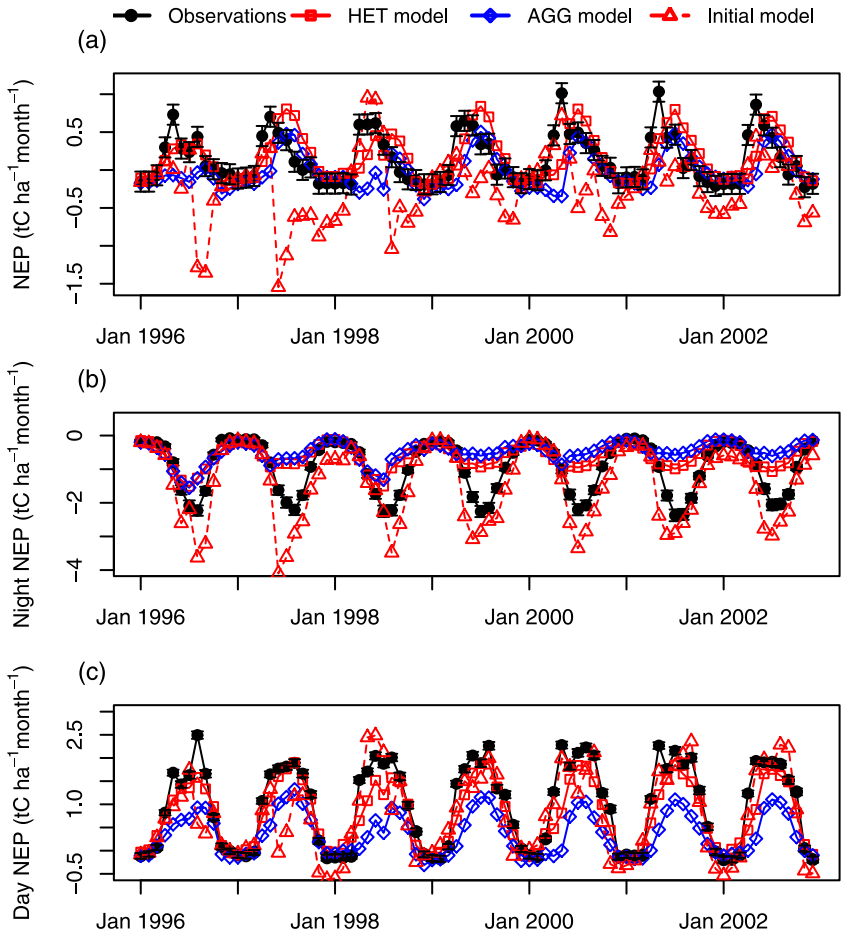

Figure 11. Monthly carbon fluxes at Howland Forest. In all panels, the black line represents the data, the solid red line indicates the predictions of the HET model, the blue line indicates the predictions of the AGG model, and the dashed red line indicates the predictions of the initial model. 2σ error bars are shown for the observations. (a) Monthly net ecosystem productivity (NEP). (b and c) Breakdown of NEP into nighttime and daytime components, respectively.

[41] The worsening of the tree growth rate bias resulted from a larger underprediction of conifer growth rates (Figure 10c), which more than offset an increase in hardwood growth rates (Figure 10d). We also ran an additional simulation that used the parameters from the HET model optimization, but aggregated the canopy in the same way as the AGG model, in order to determine whether the parameters or the representation heterogeneity was responsible for the differences in predicted growth rates. The bias in this simulation was -0.37 m^2 ha^{-1} a^{-1}, only a slight improvement over the AGG simulation, indicating that the predicted growth rates were different in HET and AGG primarily because of their different representations of heterogeneity.

[42] Seasonal patterns of carbon fluxes at Howland are shown in Figure 11. Throughout the simulated period, the monthly NEP of the HET run (RMS error of 0.29 tC ha^{-1} a^{-1}) is more realistic than that of the AGG run (RMS error of 0.37 tC ha^{-1} a^{-1}; Figure 11a). The seasonal cycle of the HET run also has the correct amplitude; however, its summertime peak in NEP lags the observed peak by approximately 2–3 months. Figures 11b and 11c show the breakdown of monthly NEP into nighttime and daytime components. Both the HET and AGG simulations underestimate respiration during summer nights, although the HET run is closer to the observations (Figure 11b). During daytime (Figure 11c), both simulations underpredict summer NEP, although the HET run's prediction (0.79 tC ha^{-1} month^{-1}) is much closer to the observations (1.00 tC ha^{-1} month^{-1}) than the AGG run's prediction (0.36 tC ha^{-1} month^{-1}).

4.3.2. Chibougamou

[43] The Chibougamou, Quebec eddy-flux tower (49.3°N, 74.0°W) is located about 770 km north of Harvard Forest (Figure 1) and is situated in a boreal ecosystem dominated by black spruce (*Picea mariana*). Because it experiences summertime mean temperatures of only 16°C and typically has an initial frost in early September, it has a shorter growing season than either Harvard or Howland. To initialize ED2 simulations of Chibougamou, we used composition data measured in 25 Quebec forest inventory plots located within 50 km of the tower site [*Penner et al.*, 1997]. HET and AGG runs were carried out for a 1-year period (2004) for which CO_2 flux measurements were available. Meteorological forcing and phenology were prescribed as for Harvard and Howland Forest sites.

[44] Figure 12 compares modeled monthly NEP with the Chibougamou data. Unlike at the Harvard and Howland sites, there is a marked decline NEP from June to July at Chibougamou. Both HET and AGG simulations capture this dip;

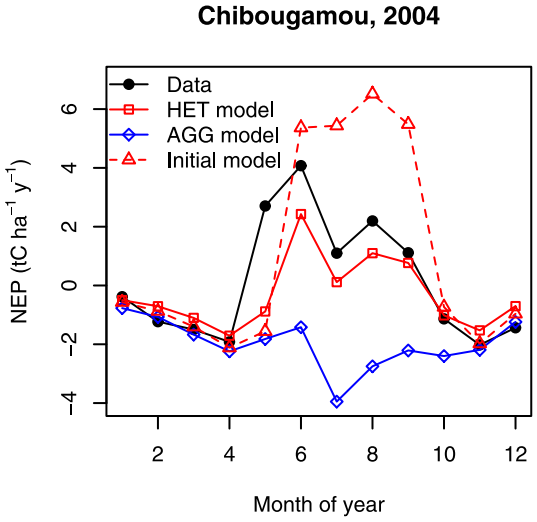

Figure 12. Monthly NEP at Chibougamou in 2004. The black line represents the measurements, the solid red line represents the HET model, the blue line represents the AGG model, and the dashed red line represents the initial model.

however, the HET run gives a better match to the observed annual NEP (AGG: −2.0 tC ha^{-1} a^{-1}, observed: 0.1 tC ha^{-1} a^{-1}, HET: −0.3 tC ha^{-1} a^{-1}). In addition, in both the observations and the HET run, the July dip in total NEP is prominent in nighttime-only NEP (not shown), indicating that ecosystem respiration is at least partly responsible for this feature.

4.3.3. Northeastern United States and Quebec

[45] All regional simulations were done on the 0.25° × 0.25° grid shown in Figure 13. Soil textural class was assigned at the level of the grid cell using the 1° resolution USDA global soil database because higher resolution data were unavailable for Quebec. Forest inventory data [*Penner et al.*, 1997; *Frayer and Furnival*, 1999], including over 27 000 plots, were used to initialize ecosystem composition. The observed pattern of above ground biomass (AGB) is shown in Figure 13a. As can be seen in the figure, the largest amounts of AGB were in northern New York, southern New England, and southern Quebec; the smallest were in western New York (because of agriculture) and northern Quebec. We then performed regional simulation the period 1982–1995 using both the HET and AGG model formulations. In both cases, the first three years were used to spin up grasses, but were then discarded from the analysis. Vegetation phenology was driven with the average phenology obtained from MODIS between 2001–2004 [*Zhang et al.*, 2003], and spatial patterns of forest harvesting (Figure 13b), derived from forest inventory data, were applied as a disturbance forcing to the model. The meteorological forcing was prescribed from the ECMWF reanalysis [*Uppala et al.*, 2005].

[46] Because most plots had been inventoried twice (once in the mid-1980s, and again in the mid-1990s), it was possible to calculate the mean rate of AGB accumulation (defined as growth minus natural mortality minus harvesting). The observed rate of AGB accumulation for these plots is shown in Figure 14a. The pattern is highly heterogeneous: New York had large accumulation rates, southern New England had smaller accumulation rates, and Maine was losing AGB. In Quebec, the accumulation rates were smaller in magnitude, with the southernmost and northernmost areas typically showing positive and negative accumulation rates, respectively.

[47] Averaged over 1985–1995, the AGG run predicted that the entire region, with the exception of northern Quebec, was a strong carbon strong sink (Figure 14b). The simulated AGB accumulation rates exceeded the observed rate everywhere except in western NY and PA. The comparison was

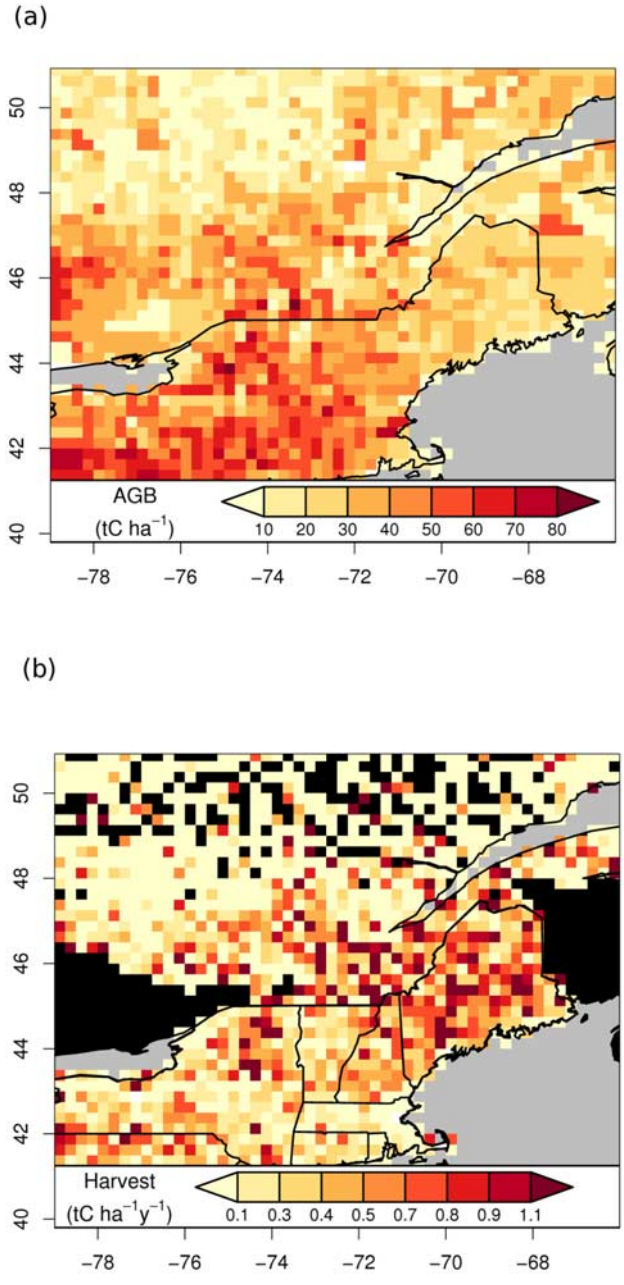

Figure 13. (a) Aboveground biomass (AGB) derived from the FIA and Quebec forest inventories aggregated at 0.25° resolution. This region included over 27 000 plots. (b) Decadal-mean harvesting rates of AGB for the forested plots. Maine, southern Quebec, and the Adirondack region experienced the largest harvesting rates of the simulated domain. Grid cells with missing data are colored black.

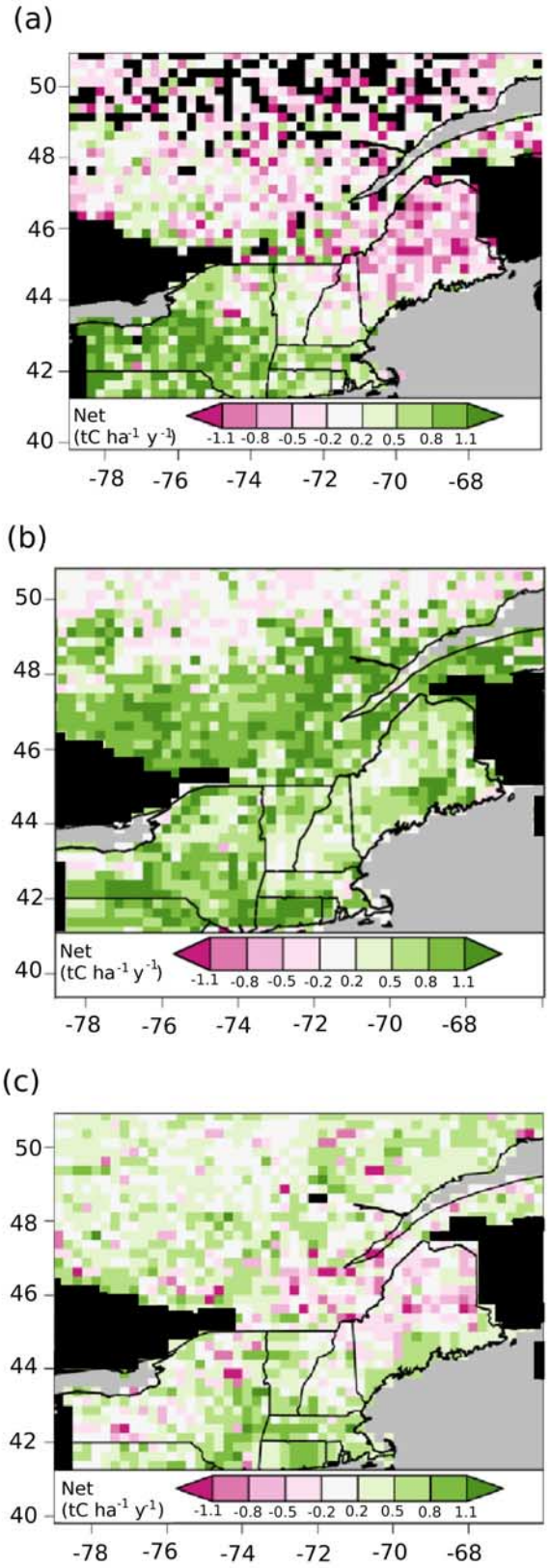

particularly bad in southern Quebec, where the overprediction was typically by about 1.5 tC ha a^{-1}. In contrast, the AGB accumulation rate predicted in the HET simulation (Figure 14c) was much more realistic, with New England and southern Quebec being a particularly good match. The HET simulation nevertheless overpredicted accumulation rates in northern Quebec, because of underprediction of mortality, and underpredicted rates in Pennsylvania and western New York, because of underprediction of growth. Overall, the mean model bias was about +40% in AGG and +5% in HET.

5. Discussion

[48] This analysis shows how ED2 can be successfully parameterized and tested against field-based measurements of ecosystem performance, yielding a terrestrial biosphere model capable of accurately predicting regional-scale variation in patterns of ecosystem carbon fluxes and vegetation dynamics over timescales of hours to decades. Using just two years of data at Harvard Forest to estimate a number of important but poorly constrained model parameters dramatically improves ED2's predictions of carbon and vegetation dynamics throughout the northeastern United States and Quebec, despite marked regional variation in meteorological forcing and ecosystem composition. These results contrast strongly with the findings of earlier studies, in which model parameter values were poorly constrained [*Braswell et al.*, 2005], or required time- and site-dependent parameters in order to obtain realistic patterns of ecosystem dynamics [*Wang et al.*, 2001; *Reichstein et al.*, 2003].

[49] The ability of ED2 to scale vegetation dynamics and carbon fluxes accurately in both time and space is in part attributable to its representation of biotic heterogeneity. In contrast to traditional models using a 'big-leaf' approximation, which seek to capture canopy-scale ecosystem dynamics by modeling the dynamics of an average plant sitting in an average environment, ED2 is structured so that it can explicitly track the dynamic, fine-scale horizontal and vertical biotic heterogeneity in canopy structure present in ecosystems even at the scale of flux-tower footprints.

[50] Consistent with results from several previous studies, our results (Table 2 and Figures 6–8) show that 'canopy-as-big-leaf' approximations that average over fine-scale biotic heterogeneity [*Knorr and Kattge*, 2005; *Wang et al.*, 2007] can yield reasonable dynamics on timescales of 2–5 years at the sites at which they have been optimized. However, as shown in Figures 10, 11, 12, and 14, 'canopy as big-leaf' representations of ecosystems have a greatly reduced ability to capture regional variation in fluxes and vegetation dynamics. This arises because the homogenization of the plant canopy that occurs in the 'big-leaf' representation results in a necessary loss of information attenuating the connections

Figure 14. Net aboveground carbon accumulation (growth minus natural mortality minus harvesting). (a) Observations from the forest inventories. The uptake is large especially in New York, while Maine had negative uptake and Quebec had near zero but slightly negative uptake. (b) Predictions of the AGG model, which generally overestimates the observations. (c) Predictions of the HET model, which nearly eliminates the overall positive bias of the AGG model.

Table 6. Covariance Matrix of the Optimized Parameters[a]

	M	$V_{mult,hw}$	$V_{mult,co}$	$T_{V,lo}$	α_{root}	q_{hw}	q_{co}	K_W	$r_{g,co}$	$\alpha_{storage,hw}$	W_{opt}	w_1	w_2	Q_{10}
M	1	−0.85	−0.93	1.0	1.3	−12	0.35	0.073	0.72	0.52	−13	−1.4	−0.37	−0.35
$V_{mult,hw}$		1	−1.4	0.39	0.61	0.51	0.23	0.19	0.44	0.85	0.33	−1.2	−1.0	−1.7
$V_{mult,co}$			1	0.71	1.5	−0.56	1.1	0.067	0.55	−1.9	1.5	−1.6	6.5	−1.2
$T_{V,lo}$				1	−0.39	4.4	−0.78	−0.13	−0.65	−0.73	−0.67	0.73	−0.36	0.47
α_{root}					1	−0.91	−0.29	−0.064	−0.37	0.24	−48	1.2	0.44	−7.0
q_{hw}						1	0.89	−0.077	0.63	−0.34	−0.26	3.0	0.44	0.70
q_{co}							1	−0.050	−0.81	−0.41	−39	−0.47	−0.65	0.89
K_W								1	−0.089	−0.15	−0.14	−0.13	0.13	0.15
$r_{g,co}$									1	−2.1	0.75	12	0.63	0.88
$\alpha_{storage,hw}$										1	−8.3	0.65	0.34	0.57
W_{opt}											1	2.1	0.19	−0.43
w_1												1	−0.20	−0.52
w_2													1	−0.21
Q_{10}														1

[a]The stomatal slope is denoted M (equation (B15)), the fine root turnover rate is denoted α_{root} (equation (C6)), the temperature at which photosynthesis begins to rapidly decline is denoted $T_{V,lo}$ (equation (B3)), the hardwood V_{m0} multiplier is denoted $V_{mult,hw}$ (equation (B3)), the allocation to fine roots relative to leaves for hardwoods is denoted q_{hw} (equation (C1)), the hardwood storage respiration rate is denoted $\alpha_{storage,hw}$ (equation (C10)), the conifer V_{m0} multiplier is denoted $V_{mult,co}$ (equation (B3)), the allocation to fine roots relative to leaves for conifers is denoted q_{co} (equation (C1)) and the conifer growth respiration fraction is denoted $r_{g,co}$ (equation (C4)). The optimal soil water is denoted W_{opt} (equation (D3)), w_1 and w_2 (equation (D3)) are parameters determining the response of the decomposition model to low and high soil moisture levels, respectively, and Q_{10} determines the response of decomposition to soil temperature (equation (D5)).

between observations and the underlying parameters of the biosphere model. As the results in Table 5 demonstrate, this loss of information and the resulting increases in parameter uncertainty occur as a result of spatial averaging of the plant canopy, and becomes even more acute when plant canopies are represented as single, dominant plant functional types.

[51] The incorporation of biotic heterogeneity in ecosystem composition and structure facilitated constraining the dynamics of both hardwoods and conifers at Harvard Forest. Because the growth and mortality rates of all plant functional types (PFTs) found within the tower footprint are predicted, the parameterizations of different PFTs were able to be simultaneously constrained using the forest inventory measurements. Optimization thus improved simulation of conifer PFTs even though they comprise only about 20% of the basal area at Harvard Forest. Importantly, we found that this improved parameterization was not site-specific, but also improved the model's ability to realistically simulate fluxes and dynamics at distant, conifer-dominated sites, including Howland Forest and Chibougamou.

[52] In addition to providing a way to distinguish conifer and hardwood dynamics, the forest inventory measurements also played a key role in constraining our predictions of canopy-scale carbon fluxes. While flux-tower measurements yield estimates of canopy scale NEP and nighttime NEP provides a measure of ecosystem respiration, these measurements do not provide insight into the partitioning of ecosystem respiration between its autotrophic and heterotrophic components. As a result, when used alone, tower-flux measurements do not constrain model predictions of net primary productivity and heterotrophic respiration, allowing models to have unrealistically high aboveground carbon accumulation rates that are compensated for by excessive rates of soil decomposition, as exemplified by the results of *Braswell et al.* [2005] (section 1). In contrast, as shown here, using flux tower observations in combination with forest inventory measurements allows accurate partitioning of total ecosystem respiration into its autotrophic and heterotrophic components, making possible realistic predictions for rates of aboveground carbon accumulation and belowground decomposition.

[53] The marked improvement in model performance following optimization at Harvard forest was associated with significant changes in a number of model parameters away from their initial, literature-prescribed values. The parameter estimates indicate higher fine-root allocation in hardwoods compared to conifers, a result that is intuitively pleasing because, on a leaf-mass basis, demand for water is higher in hardwoods than in conifers because of their higher specific leaf areas. In addition, the model fitting produces a well-constrained estimate for the rate of fine root turnover of 5.1 a^{-1}, markedly faster than the 0.33 a^{-1} value prescribed in the initial model formulation. Both of these rates of fine root turnover lie within the range of literature estimates, which indicate tremendous variation in fine root longevity, ranging from days to years, depending on root diameter [*Gaudinski et al.*, 2000; *Matamala et al.*, 2003], soil properties, and climate. This, together with the strong covariances between model parameters (Table 6), emphasizes the value of parameterizing and testing terrestrial biosphere model predictions against suites of field-based observations, rather than simply relying on hand-picked literature values to specify biosphere model parameters.

[54] Achieving consistency between the dynamics of ED2 and the flux-tower and forest inventory measurements at Harvard forest also required changes in some of the underlying submodels. Specifically, consistent with earlier terrestrial biosphere model formulations [*Foley et al.*, 1996; *Friend et al.*, 1997; *Haxeltine and Prentice*, 1996; *Knorr*, 2000], the initial model formulation assumed that one third of the carbon assimilated by the canopy is lost as growth respiration. This formulation derives from measurements of herbaceous plants [*Amthor*, 1984; *Amthor*, 2000; *van Iersel*, 2003]; however, as shown here, it is inconsistent with canopy-scale measurements of forest carbon fluxes because simulated growth respiration alone exceeds the observed rates of total ecosystem respiration at nighttime during the summer. In the alternative formulation implemented in the optimized ED2 model, hardwood growth respiration is replaced by a maintenance loss term on the storage pool, and structural tissue growth occurs at the beginning of the growing season using the carbon from the storage pool. This formulation

substantially decreases the seasonality of hardwood respiration consistent with the flux tower observations, and results in hardwood growth that is strongly seasonal in accordance with dendrometer measurements of hardwood growth (S. C. Wofsy et al., unpublished manuscript).

[55] The calculated uncertainties of the optimized parameters (Tables 5) do not explicitly include impacts of potential errors in the submodels of ED2 not directly constrained in the the optimization (e.g., the canopy and soil biophysics schemes [*Walko et al.*, 2000]). In particular, errors in predicted soil moisture may be important for capturing certain aspects of variability not currently captured by the optimized model formulation shown here.

[56] Parameter uncertainty was significantly affected by the choice of data sets used to optimize the model. In contrast to previous studies whose only metric of NEP was hourly flux data, we used hourly, monthly and annual values of NEP to constrain ED2. Although the importance of using multiple data sets has already been pointed out [*Williams et al.*, 2005], the independent constraints provided by aggregating eddy flux data in this way has not, to our knowledge, been previously exploited. We found that using these integrals of NEP doubled the number of parameters that we were able to estimate with coefficients of variation less than 25% (Appendix E). Among these were the parameters of the decomposition model, suggesting that adding the monthly and yearly timescales to the optimization increases the sensitivity to the seasonally varying fluxes into the soil carbon pools.

[57] Our analysis highlights several areas for further improvement. First, the climate-based phenology model of *Botta et al.* [2000] used in the initial model formulation significantly overestimated the length of the growing season, biasing seasonal and annual estimates of canopy carbon fluxes. We eliminated this source of error by switching to a satellite-derived prescribed phenology model; however, in order to predict how future changes in climate will alter terrestrial vegetation dynamics and carbon fluxes, there is an urgent need to develop more accurate climate-based phenology models.

[58] Second, while the optimized model accurately captured the seasonal pattern of NEP at Harvard Forest, this was not the case at Howland, where the model's summertime peak in nighttime NEP preceded the observations by 2–3 months (Figure 11c). One potential explanation for this is that either higher lignin or lower nitrogen content of the predominantly conifer litter found at Howland, compared to the predominantly hardwood litter found at Harvard, slows the onset of heterotrophic respiration at the Howland site. Alternatively, there may be differences in the environmental sensitivities of decomposition at the two sites, arising from either differences in physiological performance or differences in belowground community composition that are not captured by ED2's simple single-layer 'black-box' decomposition model.

[59] A third area for improvement is suggested by the model's overprediction of AGB accumulation in northern Quebec (Figure 14), which was due to underprediction of mortality. The model's density-independent mortality rates were calibrated solely from the FIA [*Albani et al.*, 2006], and thus did not include any Quebec data. Incorporating frost- or insect-induced mortality in accord with the Quebec observations would likely improve the match [*Kurz and Apps*, 1999]. Finally, several factors may have contributed to the underprediction of AGB accumulation and growth rates in PA and NY, although absence of direct observations makes it difficult to evaluate these hypotheses in detail. These include: (i) the impacts of nitrogen deposition, which is relatively large in PA and NY [*Goodale et al.*, 2002] but not accounted for in ED2; (ii) dependence of leaf nitrogen on relative shading, even for trees of the same PFT [*Reich et al.*, 1998; *Wright et al.*, 2004]; and (iii) a possible need to account for three-dimensional effects in ED2's radiative transfer scheme.

[60] The explicit parameter estimation and model testing conducted in this study differ from the conventional approach to evaluating terrestrial biosphere models in which models are evaluated by their ability to reproduce broad-scale patterns of vegetation and regional-scale variation in atmospheric CO_2. The ability to test the predictions of structured terrestrial biosphere models such as ED2 against field-based measurements of canopy fluxes and vegetation dynamics promises to provide much-needed empirical constraints on predictions of how changes in climate and atmospheric CO_2 will alter terrestrial ecosystems, and how these changes will feedback onto the atmosphere over the coming decades.

Appendix A: ED2 Model Overview

[61] The principal differences between ED2 and the original ED model formulation are as follows: (i) the single layer soil model (with prescribed temperature) of ED has been replaced in ED2 with a generalized version of the Land Ecosystem Atmosphere Feedback (LEAF-2) biophysical scheme [*Walko et al.*, 2000], which includes a multilayer soil model, the ability to represent liquid or frozen surface water in and above the soil, and a multilayer vegetation canopy; (ii) the computation of shortwave radiative transfer in the plant canopy was changed from an off-line, single-band, full-spectrum computation using Beer's law to an on-line, 2-band, direct-diffuse computation using the two-stream approximation; (iii) longwave radiative transfer in the plant canopy, omitted in the original ED model, was computed with the two-stream approximation in ED2; (iv) photosynthesis and evapotranspiration, done off-line in the original ED, are computed on-line in ED2 (Appendix B); (v) aerodynamic resistance, omitted in the original ED calculations of photosynthesis and evapotranspiration, is included in ED2. Thus, the resulting ED2 model formally scales fast time-scale ecosystem responses to atmospheric forcing into realistic long-term changes in ecosystem composition, structure, and function, and consistently applies the resulting feedbacks to the atmosphere.

Appendix B: Leaf Physiology

[62] ED2 uses the model of leaf-level carbon assimilation and water fluxes developed by Farquhar, Ball, Berry and others [*Farquhar et al.*, 1980; *von Caemmerer and Farquhar*, 1981; *Farquhar and Sharkey*, 1982; *Ball et al.*, 1986]. The formulation closely follows the original ED model formulation [*Moorcroft et al.*, 2001]; it is described here because several parameters in this scheme were optimized.

[63] The leaf-level carbon demand of C_3 plants is determined by the minimum of its light-limited rate (J_e) and its Rubisco-limited rate (J_c). Colimitation is not considered as this has little effect on canopy photosynthesis because, at any

given time, the fraction of leaves that are colimited is small. Thus, the optimal leaf-level demand of photosynthesis is given by

$$A_o = \min(J_e, J_c) - \gamma V_m(T_v) \text{open stomata} \tag{B1}$$

$$A_c = -\gamma V_m(T_v) \text{ closed stomata} \tag{B2}$$

where the term $-\gamma V_m$ represents leaf respiration. $V_m(T_v)$ denotes here the maximum capacity of Rubisco to perform the carboxylase function at a given temperature T_v and γ is a proportionality constant [*Reich et al.*, 1998]. The temperature dependence of $V_m(T_v)$ is exponential, but a phenomenological cutoff is applied at very low and very high temperatures. At low temperatures, this cutoff is governed by the parameter $T_{V,lo}$. Thus we have, for the unoptimized model,

$$V_m(T_v) = \frac{V_{m0,i} \exp 3000(1/288.15 - 1/T_v)}{\left(1 + \exp 0.4\left(T_{V,lo} - T_v\right)\right)(1 + \exp 0.4(T_v - 318.15))}. \tag{B3}$$

[64] The optimized model ramps down photosynthesis in the fall [*Wilson et al.*, 2000] through a modification of V_m,

$$V_m(T_v) = V_{m0,i} \cdot \frac{\exp 3000(1/288.15 - 1/T_v)}{\left(1 + \exp 0.4\left(T_{V,lo} - T_v\right)\right)(1 + \exp 0.4(T_v - 318.15))} \cdot \frac{e(1.09t)}{e(t)}, \tag{B4}$$

where t is the day of the year and $e(t)$ is defined by

$$e(t) = \frac{1}{1 + (t/t_0)^b}, \tag{B5}$$

where t_0 is the mean, b is a slope, and t is the Julian day. The parameters t_0 and b were obtained from fits to four key dates derived from MODIS phenology observations [*Zhang et al.*, 2003]; see section 3.1.

[65] The light-limited rate of photosynthesis is given by:

$$J_e = \alpha \text{PAR}_{vi} \frac{C_{inter} - \Gamma}{C_{inter} + 2\Gamma}, \tag{B6}$$

where α is the quantum efficiency, PAR_v is the PAR absorbed by the vegetation layer, C_{inter} is the intercellular CO_2 concentration, and Γ is the compensation point for gross photosynthesis given by:

$$\Gamma = (21.2 \text{ ppmv}) \exp(5000[1/288.15 - 1/T_v]). \tag{B7}$$

[66] The Rubisco-limited CO_2 demand is

$$J_c = \frac{V_m(T_v)(C_{inter} - \Gamma)}{C_{inter} + K_1(1 + K_2)}, \tag{B8}$$

where K_1 is the Michaelis-Menten coefficient for CO_2 and K_2 is proportional to the Michaelis-Menten coefficient for O_2. These are given by:

$$\begin{aligned} K_1 &= 150 \text{ ppmv } \exp(6000(1/288.15 - 1/T_v)) \\ K_2 &= 0.836 \exp(-1400(1/288.15 - 1/T_v)). \end{aligned} \tag{B9}$$

[67] When a plant is actively photosynthesizing, C_{inter} will generally be much less than the CO_2 concentration of the canopy air space, here denoted χ_{CAS}, because of aerodynamic and stomatal resistance. The aerodynamic resistance is mainly controlled by environmental factors like wind speed and leaf shape. The total boundary layer conductance for H_2O exchange (g_{bH}) is the sum of the conductance from free (g_{bHf}) and from forced (g_{bHw}) convection. Following *Monteith* [1973] and *Leuning et al.* [1995], we represent these conductances as

$$\begin{aligned} g_{bHw} &= (0.003 \text{ s}^{1.5} \text{ m}^{-1}) \sqrt{U/w_{leaf}} \\ g_{bHf} &= \left(0.5 \text{ s}^2 \text{ K}^{0.25} \text{ m}^{2.75}\right) D_H Gr^{0.25} w_{leaf}^{-1}. \end{aligned} \tag{B10}$$

Here, U is the wind speed and declines exponentially with the cumulative LAI (LAI_{cumul}) according to

$$U = U_{top} \exp(-0.5 \text{LAI}_{cumul}), \tag{B11}$$

where Gr is the Grashof number,

$$Gr = 1.6 \times 10^8 |T_v - T_{CAS}| w_{leaf}^3, \tag{B12}$$

and w_{leaf} is the leaf width and D_H is the molecular diffusivity for heat. For water vapor, the boundary layer conductance is given by $g_{bw} = 1.075 g_{bH}$. Water and CO_2 concentrations within the within the leaf boundary layer (e_S and C_S, respectively) are then given by

$$e_S = e_a + \frac{\Psi_o}{g_{bw}} \tag{B13}$$

and

$$C_S = \chi_{CAS} - \frac{A_o}{1.4 g_{bw}}, \tag{B14}$$

where e_a is the molar mixing ratio of water in the canopy air space (CAS).

[68] Stomatal resistance is actively regulated by the plant to control water losses. *Leuning* [1995] has shown that the connection between the stomatal conductance for water (g_{sw}) and the CO_2 assimilation rate can be expressed as

$$g_{sw} = \begin{cases} \frac{MA_o}{(C_s - \Gamma)\left(1 + \frac{D_s}{D_0}\right)} + b & \text{for open stomata,} \\ b & \text{for closed stomata.} \end{cases} \tag{B15}$$

Here, M and D_0 are empirical constants and b is the cuticular conductance. D_s represents the water vapor deficit ($D_s = e_L - e_S$) and e_L is the intercellular water vapor

concentration, assumed to be at saturation. First-order diffusion equations are also used to relate intercellular and boundary layer mixing ratios for H_2O and CO_2,

$$e_L = e_S + \frac{\Psi_o}{g_{sw}} \tag{B16}$$

$$C_{inter} = C_S - \frac{A_o}{1.6 g_{sw}}. \tag{B17}$$

[69] In contrast to terrestrial ecosystem models such as the original ED model that require an energy balance equation to determine the leaf temperature T_v, in ED2 T_v is a prognostic variable calculated by surface energy balance submodel [*Walko et al.*, 2000]. Because g_{bw}, χ_{CAS}, e_a and e_L are not coupled to the rest of the equations they can be directly determined. Then, given the known foliar temperature T_v, we are left with 6 equations in the case of open stomata (equations (B2), (B13)–(B17)) that are solved for the 6 unknowns: g_{sw}, C_S, e_s, C_{inter}, A_o and Ψ_o. In ED2, the equations are reduced to a single polynomial that is solved for the above quantities [*Medvigy*, 2006].

[70] After solving equations (B2) and (B13)–(B17) under the condition of open stomata, the equations are resolved under the condition of closed stomata by setting the stomatal conductance equal to the cuticular conductance b (equation (B15)), yielding the values for the closed-stomata leaf-level CO_2 and H_2O fluxes, A_c and Ψ_c.

[71] Water limitation: The instantaneous rates of photosynthesis A_{net} and evapotranspiration of plants Ψ_{net} rates are influenced by water availability. A_{net} and Ψ_{net} are taken to be a linear combinations of their rates under conditions of open (A_o, Ψ_o) and closed (A_c, Ψ_c) stomata, the weighting of being determined by a plant's water availability relative to its overall water demand:

$$A_{net} = f_{o,w} A_o + \left(1 - f_{o,w}\right) A_c, \tag{B18}$$

$$\Psi_{net} = f_{o,w} \Psi_o + \left(1 - f_{o,w}\right) \Psi_c, \tag{B19}$$

where the weighting for open stomata ($f_{o,w}$) is given by:

$$f_{o,w} = \frac{1}{1 + \frac{\text{Demand}}{\text{Supply}}}. \tag{B20}$$

The plant's water demand is given by:

$$\text{Demand} = \Psi_o \ \text{SLA} \ B_{leaf}. \tag{B21}$$

where SLA is the plant's specific leaf area and B_{leaf} is the plant's the leaf biomass. The plant's water availability is calculated as:

$$\text{Supply} = K_W \ W_{avail,tot} \ B_{root}, \tag{B22}$$

where the total amount of water accessible to the vegetation layer is $W_{avail,tot}$, the vegetation layer's total C in fine roots is B_{root}, and K_W is a constant.

Appendix C: Allocation

[72] Allocation in the optimized ED2 model differs from the original ED model [*Moorcroft et al.*, 2001] and is described here. The active biomass pool (B_a) of each vegetation layer consists of leaves (B_{leaf}), fine roots (B_{root}), sapwood (B_{sw}) and a stored leaf pool (B_{slc}). These are obtained through the allocation relationships

$$\begin{aligned} B_{leaf} &= \frac{e(t) B_a}{1 + q + q_{sw} h} \\ B_{root} &= \frac{q B_a}{1 + q + q_{sw} h} \\ B_{sw} &= \frac{q_{sw} h B_a}{1 + q + q_{sw} h} \\ B_{slc} &= \frac{\left(1 - e(t)\right) B_a}{1 + q + q_{sw} h} \end{aligned} \tag{C1}$$

Here, $e(t)$ is a factor ranging between 0 and 1 that accounted for phenological status of the plant (see equation (B5)). The allocation to fine roots relative to leaves, q, is PFT-dependent; q_{co} (conifers) and q_{hw} (hardwoods) were determined by the optimization.

C1. Active Biomass Pool

[73] The active biomass pool (B_a) of each vegetation layer evolves according to:

$$\frac{dB_a}{dt} = \underbrace{\theta_1 \left(\text{GPP} - R_{leaf} - R_{root} - R_{growth} - F_{litter}\right)}_{\text{photosynthesis,respiration,litter flux}} + \underbrace{\theta_2 \tau \left(B_a^* - B_a\right)}_{\text{transfer from storage}} - \underbrace{R_{slc}}_{\text{respiration of stored leaf carbon}}. \tag{C2}$$

The parameter θ_1 is either equal to 0 or 1; it is 1 if either the sum of the contributions from photosynthesis (GPP), respiration (R_{leaf}, R_{root}, R_{growth}) and litter (F_{litter}) is less than zero (GPP $- R_{leaf} - R_{root} - R_{storage} - F_{litter} < 0$), or if the vegetation layer is off-allometry with $B_a < B_a^*$. B_a^* is maximum allowable value of B_a and is calculated based on the vegetation layer's PFT and DBH through

$$B_a^* = (1 + q_r + h q_{sw}) l_1 \min\left(\frac{\text{DBH}}{\text{cm}}, \frac{\text{DBH}_0}{\text{cm}}\right)^{l_2}, \tag{C3}$$

where h is the height of the vegetation layer and q_r, q_{sw}, l_1, DBH_0 and l_2 are PFT-dependent constants (Table 3).

[74] Growth respiration (R_{growth}) was updated daily and based on the previous day's carbon balance. It is given by:

$$R_{growth} = \max\left(0, r_g \int_{\text{previous day}} dt \left(\text{GPP} - R_{leaf} - R_{root}\right)\right). \tag{C4}$$

where r_g is a PFT-dependent constant.

[75] The litter flux (F_{litter}) receives inputs from the turnover of fine roots (T_{root}), turnover of leaves from needleleaf trees (T_{leaf}) and hardwoods' dropping of leaves (T_{drop}):

$$F_{litter,i} = T_{drop} + T_{leaf} + T_{root}. \tag{C5}$$

Following *Moorcroft et al.* [2001], a plant's fine root turnover rate is given by

$$T_{root} = \alpha_{root} B_{root} \left[1 + \exp 0.4\left(278.15 - T_{g_{N_g}}\right)\right]^{-1}, \tag{C6}$$

where α_{root} is the intrinsic rate of fine root turnover.

[76] The turnover rate of the leaves of evergreen trees (T_{leaf}) is

$$T_{leaf} = \alpha_{leaf} B_{leaf} \tag{C7}$$

where α_{leaf} is a PFT-dependent constant and B_{leaf} is the size of the leaf biomass pool (Appendix C). As deciduous trees lose their leaves at the end of the growing season (section 3.1), a fraction L_{frac} of the leaf biomass is incorporated into the storage pool ($B_{storage}$; see below) and the remainder, T_{drop}, contributes to the litter flux (F_{litter}; equation (C5)).

[77] The second term in equation (C2) represents transfer from storage ($B_{storage}$) to B_a. θ_2 is a parameter equal to either 0 or 1, and is 1 only if both the vegetation layer is flushing ($de(t)/dt > 0$; equation (B5)) and off-allometry ($B_a < B_a^*$). τ is a constant equal to 1 d^{-1}.

[78] Finally, the stored leaf pool turns over at a rate given by $\alpha_{storage}$; thus,

$$R_{slc} = \alpha_{storage} B_{slc}, \tag{C8}$$

where $\alpha_{storage}$ is a constant (Table 5) and B_{slc} is the size of the stored leaf pool.

C2. Storage Pool

[79] The storage biomass pool ($B_{storage}$) of each vegetation layer evolves according to:

$$\frac{dB_{storage}}{dt} = \underbrace{(1-\theta_1)(\mathrm{GPP} - R_{leaf} - R_{root} - R_{growth} - F_{litter})}_{\text{photosynthesis,respiration,litter flux}} - \underbrace{\theta_2 \tau \left(B_a^* - B_a\right)}_{\text{transfer to active pool}} - \underbrace{R_{storage}}_{\text{respiration of storage pool}} + \underbrace{\frac{L_{frac}}{1-L_{frac}} T_{drop}}_{\text{transfer at leaf drop}}. \tag{C9}$$

Storage respiration ($R_{storage}$) depends on the current size of the storage biomass ($B_{storage}$) and is calculated daily according to

$$R_{storage} = \alpha_{storage} B_{storage} \tag{C10}$$

where $\alpha_{storage}$ is a constant (Table 5). In contrast to growth respiration, which is only operative during the growing season when daily carbon uptake is positive, storage respiration occurs throughout the year provided $B_{storage}$ is nonzero. In the initial model formulation hardwood r_g = 0.333 and hardwood $\alpha_{storage}$ is zero, while in the optimized model formulation hardwood r_g is zero and hardwood $\alpha_{storage} > 0$.

Appendix D: Soil Decomposition Model

[80] Except for the differences noted in this section, decomposition in ED2 exactly follows the original ED model [*Moorcroft et al.*, 2001]. The overall rate of decomposition is proportional to a phenomenological factor (A; 0–1) accounting for the temperature and moisture dependence of heterotrophic respiration. Two formulations for A are included in the model, the first of which exactly follows *Moorcroft et al.* [2001]. Defining

$$x_T = \left(T_{resp,\max} - T\right)\left(T_{resp,\max} - T_{resp,opt}\right)^{-1}, \tag{D1}$$

$$x_W = WW_{sat}^{-1} \tag{D2}$$

and

$$f(x_W) = \begin{cases} \exp\left[\left(x_W - W_{opt}\right)w_1\right] & x_W < W_{opt} \\ \exp\left[\left(W_{opt} - x_W\right)w_2\right] & x_W > W_{opt} \end{cases}, \tag{D3}$$

A is given by

$$A = x_T^{t_{shr}} \exp\left[t_{shr} t_{shl}^{-1}\left(1 - x_T^{t_{shl}}\right)\right] f(x_W). \tag{D4}$$

[81] The second and simpler way uses the same formulation for $f(x_W)$ but replaces the temperature dependence of equation (D4) with a simple exponential,

$$f(x_T) = \exp\left[\frac{\log Q_{10}}{10}(T - 318.15)\right]. \tag{D5}$$

Appendix E: Model Fitting Procedure

E1. Uncertainty Analysis

[82] The shape of the log-likelihood function in the neighborhood of the maximum contains information pertaining to parameter uncertainty and covariances between model parameters. When there are many parameters being optimized it is impossible to consider the log-likelihood function (equation (1)) comprehensively, but it can be shown that it is valid to consider projections of the log-likelihood function provided it is nearly quadratic near the maximum [*Edwards*, 1972]. Denote the vector of evaluates by $\hat{\theta}$ and then consider a different vector, θ, for which all but one of the components are the same as those of $\hat{\theta}$. For a fixed m, the hyper-ellipsoid given by

$$m = S\left(\hat{\theta}\right) - S(\theta) \tag{E1}$$

is defined as the m-unit log-likelihood region. We can associate some meaning with m by Taylor-expanding the log-likelihood around $\hat{\theta}$ and dropping all terms beyond the quadratic. In the one-dimensional case,

$$S_2(\theta) = S\left(\hat{\theta}\right) - \frac{1}{2}\left(\frac{\theta - \hat{\theta}}{w_\theta}\right)^2, \tag{E2}$$

Table E1. Parameter Values and Uncertainties Resulting From Three Different Optimizations[a]

Parameter	Initial Value	Optimized Value and 2σ Uncertainty		
		Hourly Only	Hourly + Yearly	Hourly + Yearly + Monthly
Stomatal Slope	8	11 (80)	8.2 (5.0)	6.4 (1.3)
Hardwood V_{m0} multiplier	1	0.90 (0.2)	1.3 (0.09)	1.1 (0.08)
Conifer V_{m0} multiplier	1	0.54 (0.10)	0.58 (0.09)	0.73 (0.1)
Photosynthesis temperature threshold (°C)	5	3.8 (3.8)	4.6 (2.7)	4.7 (2.3)
Fine root turnover rate (a^{-1})	0.333	2.6 (0.3)	5.9 (0.7)	5.1 (0.5)
Allocation to fine roots relative to leaves, hardwoods	1	1.8 (0.9)	0.9 (0.2)	1.1 (0.2)
Allocation to fine roots relative to leaves, conifers	1	0.56 (0.15)	0.24 (0.07)	0.35 (0.07)
Water availability parameter ($m^2\ a^{-1}$ (kgC root)$^{-1}$)	160	80 (810)	220 (400)	150 (1200)
Conifer growth respiration fraction	0.333	0.46 (0.08)	0.46 (0.07)	0.45 (0.06)
Hardwood growth respiration fraction	0.333	-	-	-
Hardwood storage respiration rate (a^{-1})	-	0.62 (0.17)	0.67 (0.08)	0.62 (0.08)
Optimal temperature (°C)	35	-	-	-
Temperature convexity parameter	0.19	-	-	-
Temperature convexity parameter	1.8	-	-	-
Optimal soil moisture ($m^3\ m^{-3}$)	0.6	0.94 (3.5)	0.89 (0.05)	0.89 (0.04)
Soil moisture convexity parameter	5.0	4 (336)	5.2 (1.9)	5.1 (1.8)
Soil moisture convexity parameter	5.6	5 (237)	4.8 (7.2)	4.5 (5.8)
Temperature Q_{10}	-	3.0 (90)	2.2 (0.1)	2.1 (0.09)

[a]All optimizations included the forest inventory and hourly evapotranspiration data sets. In addition, the 'Hourly only' optimization included hourly NEP data, the 'Hourly + Yearly' included hourly and yearly NEP data, and the 'Hourly + Yearly + Monthly' included hourly, yearly and monthly NEP data. Including the yearly and monthly NEP data substantially reduces parameter uncertainty.

where $S_2(\theta)$ now denotes the quadratic approximation to $S(\theta)$. The parameter $w\theta$, known as the span, is simply related to the second derivative of $S(\theta)$ about the maximum and plays the role of the standard deviation. When $\theta = \hat{\theta} + 2\ w\theta$, $m = 2$; this is the value of θ used for the estimate of parameter uncertainty (Table 5).

[83] The case of multiple parameters is similar. The Taylor expansion is written

$$S_2(\theta) = S\left(\hat{\theta}\right) - \frac{1}{2}\left(\theta - \hat{\theta}\right)' B\left(\theta - \hat{\theta}\right), \tag{E3}$$

where θ and $\hat{\theta}$ are now vectors of parameters and B is the matrix of second-order partial derivatives of $S(\theta)$ evaluated at $\hat{\theta}$. The inverse of B is known as the formation matrix. The diagonal elements are the squared spans of the corresponding parameters, and the off-diagonal elements are known as the coformations. Denoting the spans of parameters i and j to be w_i and w_j, and their coformation to be C_{ij}, a nondimensional measure of covariance is $C_{ij}/(w_i w_j)$.

[84] These covariances between parameter values are given in Table 6. Of the 91 independent covariances, 65 have magnitudes less than 1. This indicates that the projection of the support function onto the corresponding two-dimensional parameter space is parabolic, and that the second-order Taylor expansion of the support function about the optimal parameters is appropriate. Covariances having magnitudes greater than 1 result when the two-dimensional projection of the support function is hyperbolic; third or higher order Taylor expansions of the support function are necessary to assess correlations between such pairs of parameters.

[85] The maximum photosynthetic rate for hardwoods ($V_{mult,hw}$) is correlated with the turnover rate of stored carbon ($\alpha_{storage,hw}$) and is anticorrelated with the stomatal conductance-photosynthesis parameter M. The maximum photosynthetic rate for conifers ($V_{mult,co}$) is also anticorrelated with M, and also correlated with photosynthesis temperature threshold $T_{V,lo}$. The turnover rate of fine roots (α_{root}) is anticorrelated with the hardwood fine root to leaf ratio (q_{hw}), while q_{hw} is correlated with q_{co} and anticorrelated with Q_{10}. q_{co} is anticorrelated with the conifer growth respiration fraction $r_{g,co}$ and $T_{V,lo}$ and correlated with Q_{10}. $\alpha_{hw,storage}$ is correlated with $T_{V,lo}$. $r_{g,co}$ is correlated with the optimum soil moisture for decomposition W_{opt}, Q_{10} and M. W_{opt} is anticorrelated with $T_{V,lo}$. $T_{V,lo}$ with correlated with w_1, the shape parameter for the moisture dependence of heterotrophic respiration. Other parameter pairs were either more weakly covarying or resulted in hyperbolic fits to the support function.

[86] To address higher-order covariances among the optimized parameters we also performed a principal components analysis [*Draper and Smith*, 1981]. The eigenvector corresponding to the highest eigenvalue was interpretable, and indicated that the goodness of fit function varied most strongly in the direction of changing net primary productivity.

E2. Selection of Eddy Flux Tower Data Sets

[87] Previous analyses using eddy flux tower data employed only hourly time-scale data in constructing their likelihood functions. However, it is possible to do reasonably well in predicting hourly fluxes but to nevertheless have a systematic error that leads to erroneous monthly and yearly fluxes. This is illustrated in Table E1, which shows the parameters and uncertainties resulting from 3 different ED2 optimizations. Represented are the study described in this manuscript that used hourly, monthly and yearly fluxes; a second optimization that did not include monthly fluxes but had hourly and yearly fluxes; and a third optimization that included hourly fluxes but neither monthly nor yearly fluxes. All optimizations included the forest inventory data sets and the hourly evapotranspiration data.

[88] Parameter uncertainty was substantially decreased when yearly fluxes were included in the optimization. While the optimization using only hourly flux data yielded only 6 of 14 parameters with coefficients of variation less than 25%, the optimization that also included yearly fluxes had 10 such parameters. These 10 parameters included all of the 6 from the hourly flux-only optimization, plus q_{hw}, W_{opt}, w_1 and Q_{10}. Thus, the heterotrophic respiration model particularly

responded to the annual-scale fluxes. Adding monthly fluxes further improved the optimization, yielding 12 parameters with coefficients of the variation less than 25%; the additional parameters were M and $T_{V,lo}$.

[89] **Acknowledgments.** P. R. Moorcroft, S. C. Wofsy, J. W. Munger, and D. Y. Hollinger gratefully acknowledge funding from the National Science Foundation BE/CBC Program grant ATM-0221850 and BE program grant ATM-0450307. P. R. Moorcroft, S. C. Wofsy, and J. W. Munger also acknowledge funding from the Harvard Forest LTER, and from the Office of Science, Biological and Environmental Research Program (BER) of the U.S. Department of Energy, through the northeast regional center of the National Institute for Global Environmental Change (NIGEC) and through the northeastern region of the National Institute for Climatic Change Research (NICCR) under cooperative agreement DE-FC02-03ER63613. Measurements at the Harvard Forest site are supported by the BER through the NICCR (DE-FC02-06ER64157) and the Terrestrial Carbon Program (DE-FG02-07ER64358). The authors also thank Mark Friedl and Tan Bin for their assistance and generosity in providing the MODIS-derived leaf onset and offset dates used in the prescribed phenology model. NCEP Reanalysis data provided by the NOAA/OAR/ESRL PSD, Boulder, Colorado, USA, from their Web site at http://www.cdc.noaa.gov/.

References

Albani, M., D. Medvigy, G. C. Hurtt, and P. R. Moorcroft (2006), The contributions of land-use change, CO_2 fertilization, and climate variability to the eastern U.S. carbon sink, *Global Change Biol.*, *12*, 2370–2390.

Amthor, J. S. (1984), The role of maintenance respiration in plant growth, *Plant Cell Environ.*, *7*, 561–569.

Amthor, J. S. (2000), The McCree-de Wit-Penning de Vries-Thornley respiration paradigms: 30 years later, *Ann. Bot. London*, *86*, 1–20.

Baldocchi, D., et al. (1996), Strategies for measuring and modelling carbon dioxide and water vapour vluxes over terrestrial ecosystems, *Global Change Biol.*, *2*, 159–168.

Ball, J. T., I. E. Woodrow, and J. A. Berry (1986), A model predicting stomatal conductance and its contribution to the control of photosynthesis under different environmental conditions, in *Progress in Photosynthesis Research*, edited by I. Biggins, pp. 221–224, Martinus Nijhoff, Netherlands.

Barford, C. C., et al. (2001), Factors controlling long- and short-term sequestration of atmospheric CO_2 in a mid-latitude forest, *Science*, *294*, 1688–1691.

Botkin, D. B., J. F. Janak, and J. R. Wallis (1972), Rationale, limitations, and assumptions of a northeastern forest growth simulator, *IBM J. Res. Dev.*, *16*, 101–116.

Botta, A., N. Viovy, P. Ciais, P. Friedlingstein, and P. Monfray (2000), A global prognostic scheme of leaf onset using satellite data, *Global Change Biol.*, *6*, 709–725.

Braswell, B. H., W. J. Sacks, E. Linder, and D. S. Schimel (2005), Estimating diurnal to annual ecosystem parameters by synthesis of a carbon flux model with eddy covariance net ecosystem exchange observations, *Global Change Biol.*, *11*, 335–355.

Cramer, W., et al. (2001), Global response of terrestrial ecosystem structure and function to CO_2 and climate change: Results from six dynamic global vegetation models, *Global Change Biol.*, *7*, 357–373.

Denman, K. L., et al. (2007), Couplings between changes in the climate system and biogeochemistry, in *Climate Change 2007: The Physical Science Basis. Contribution of Working Group I to the Fourth Assessment Report of the Intergovernmental Panel on Climate Change*, edited by S. Solomon et al., Cambridge Univ. Press, Cambridge.

Draper, N. R., and H. Smith (1981), *Applied Regression Analysis*, John Wiley, New York.

Dufresne, J.-L., et al. (2002), On the magnitude of positive feedback between future climate change and the carbon cycle, *Geophys. Res. Lett.*, *29*(10), 1405, doi:10.1029/2001GL013777.

Edwards, A. W. F. (1972), *Likelihood*, Cambridge Univ. Press, Cambridge.

Farquhar, G. D., and T. D. Sharkey (1982), Stomatal conductance and photosynthesis, *Ann. Rev. Plant Physiol.*, *33*, 317–345.

Farquhar, G. D., S. von Caemmerer, and J. A. Berry (1980), A biochemical model of photosynthetic CO_2 assimilation in leaves of C_3 species, *Planta*, *149*, 78–90.

Foley, J. A., I. C. Prentice, N. Ramankutty, S. Levis, D. Pollard, S. Sitch, and A. Haxeltine (1996), An integrated biosphere model of land surface processes, terrestrial carbon balance, and vegetation dynamics, *Global Biogeochem. Cycles*, *10*, 603–628.

Frayer, W. E., and G. M. Furnival (1999), Forest survey sampling designs: A history, *J. For.*, *97*, 4–10.

Friedlingstein, P., et al. (2006), Climate-carbon feedback analysis: Results from the C4MIP model intercomparison, *J. Clim.*, *19*, 3337–3353.

Friend, A. D., A. K. Stevens, R. G. Knox, and M. G. R. Cannell (1997), A process-based, terrestrial biosphere model of ecosystem dynamics (Hybrid v3.0), *Ecol. Model.*, *95*, 249–287.

Gaudinski, J. B., S. E. Trumbore, E. A. Davidson, and S. Zheng (2000), Soil carbon cycling in a temperate forest: Radiocarbon-based estimates of residence times, sequestration rates and partitioning of fluxes, *Biogeochemistry*, *51*, 33–69.

Goodale, C. L., K. Lajtha, K. J. Nadelhoffer, E. W. Boyer, and N. A. Jaworski (2002), Forest nitrogen sinks in large eastern U. S. watersheds: Estimates from forest inventory and an ecosystem model, *Biogeochemistry*, *57/58*, 239–266.

Haxeltine, A., and I. C. Prentice (1996), Biome 3: An equilibrium terrestrial biosphere model based on ecophysiological constraints, resource availability, and competition among plant functional types, *Global Biogeochem. Cycles*, *10*, 693–709.

Hollinger, D. Y., and A. D. Richardson (2005), Uncertainty in eddy covariance measurements and its application to physiological models, *Tree Physiol.*, *25*, 873–885.

Hollinger, D. Y., S. M. Goltz, E. A. Davidson, J. T. Lee, K. Tu, and H. T. Valentine (1999), Seasonal patterns and environmental control of carbon dioxide and water vapour exchange in an ecotonal boreal forest, *Global Change Biol.*, *5*, 891–902.

Hollinger, D. Y., et al. (2004), Spatial and temporal variability in forest-atmosphere CO_2 exchange, *Global Change Biol.*, *10*, 1689–1706.

Hurtt, G. C., P. R. Moorcroft, S. W. Pacala, and S. A. Levin (1998), Terrestrial models and global change: Challenges for the future, *Global Change Biol.*, *4*, 581–590.

Huston, M. (1992), Individual-based forest succession models and the theory of plant competition, in *Individual-Based Models and Approaches in Ecology*, edited by D. L. DeAngelis and L. J. Gross, pp. 408–420, Chapman and Hall, London, UK.

Huston, M. A., D. L. DeAngelis, and W. M. Post (1988), New computer models unify ecological theory, *Bioscience*, *38*, 682–691.

Kalnay, E., et al. (1996), The NCEP/NCAR 40-year reanalysis project, *Bull. Am. Meteorol. Soc.*, *77*, 437–470.

Knorr, W. (2000), Annual and interannual CO_2 exchanges of the terrestrial biosphere: Process-based simulations and uncertainties, *Global Ecol. Biogeogr.*, *9*, 225–252.

Knorr, W., and J. Kattge (2005), Inversion of terrestrial ecosystem model parameter values against eddy covariance measurements by Monte Carlo sampling, *Global Change Biol.*, *11*, 1333–1351.

Kurz, W. A., and M. J. Apps (1999), A 70-year retrospective analysis of carbon fluxes in the Canadian forest sector, *Ecol. Appl.*, *9*, 526–547.

Leuning, R. (1995), A critical appraisal of a combined stomatal-photosynthesis model for C_3 plants, *Plant Cell Environ.*, *18*, 339–355.

Leuning, R., F. M. Kelliher, D. G. G. de Pury, and E.-D. Schulze (1995), Leaf nitrogen, photosynthesis, conductance and transpiration: Scaling from leaves to canopies, *Plant Cell Environ.*, *18*, 1183–1200.

Levin, S. A., et al. (1997), Mathematical and computational challenges in population biology and ecosystems science, *Science*, *275*, 334–343.

Mahadevan, P., et al. (2008), A satellite-based biosphere parameterization for net ecosystem CO_2 exchange: Vegetation Photosynthesis and Respiration Model (VPRM), *Global Biogeochem. Cycles*, *22*, GB2005, doi:10.1029/2006GB002735.

Matamala, R., M. A. Gonzàlez-Meler, J. D. Jastrow, R. J. Norby, and W. H. Schlesinger (2003), Impacts of fine root turnover on forest NPP and soil C sequestration potential, *Science*, *302*, 1385–1387.

Medvigy, D. M. (2006), The state of the regional carbon cycle: Results from a coupled constrained ecosystem-atmosphere model, Ph.D. thesis, Harvard Univ., Cambridge, Mass.

Melillo, J. M., et al. (1995), Vegetation/ecosystem modeling and analysis project: Comparing biogeography and biogeochemistry models in a continental-scale study of terrestrial ecosystem responses to climate change and CO_2 doubling, *Global Biogeochem. Cycles*, *9*, 407–437.

Miller, D. A., and R. A. White (1998), A conterminous United States multilayer soil characteristics data set for regional climate and hydrology modeling, *Earth Interactions*, *2*, 1–26.

Monteith, J. L. (1973), *Principles of Environmental Physics*, Edward Arnold, London.

Moorcroft, P. R. (2003), Recent advances in ecosystem-atmosphere interactions: An ecological perspective, *Proc. R. Soc. London, Ser. B*, *B270*, 1215–1227.

Moorcroft, P. R. (2006), How close are we to a predictive science of the biosphere?, *Trends Ecol. Evol.*, *21*, 400–407.

Moorcroft, P. R., G. C. Hurtt, and S. W. Pacala (2001), A method for scaling vegetation dynamics: The Ecosystem Demography model (ED), *Ecol. Monogr.*, *71*, 557–586.

Pacala, S. W., C. D. Canham, J. Saponara, J. A. Silander Jr., R. K. Kobe, and E. Ribbens (1996), Forest models defined by field measurements: Estimation, error analysis and dynamics, *Ecol. Monogr.*, *66*, 1–43.

Paembonan, S. A., A. Hagihara, and K. Hozumi (1992), Long-term respiration in relation to growth and maintenance processes of the aboveground parts of a hinoki forest tree, *Tree Physiol.*, *10*, 101–110.

Penner, M., K. Power, C. Muhairwe, R. Tellier, and Y. Wang (1997), Canadas forest biomass resources: Deriving estimates from Canadas forest inventory, *Inf. Rep. BC-X-370*, Nat. Resour. Can., Can. For. Serv., Pac. For. Cent., Victoria, B. C., Canada.

Press, W. H., S. A. Teukolsky, W. T. Vetterling, and B. P. Flannery (1992), *Numerical Recipes in C: The Art of Scientific Computing*, Cambridge Univ. Press, Cambridge.

Rastetter, E. B., A. W. King, B. J. Cosby, G. M. Hornberger, R. V. ONeill, and J. E. Hobbie (1992), Aggregating fine-scale ecological knowledge to model coarser-scale attributes of ecosystems, *Ecol. Appl.*, *2*, 55–70.

Raupach, M., P. Rayner, D. Barrett, R. DeFries, M. Heimann, D. Ojima, S. Quegan, and C. Schmullius (2005), Model-data synthesis in terrestrial carbon observation: Methods, data requirements and data uncertainty specifications, *Global Change Biol.*, *11*, 378–397, doi:10.1111/j.1365-2486.2005.00917x.

Reich, P. B., M. B. Walters, D. S. Ellsworth, J. M. Vose, J. C. Volin, C. Gresham, and W. D. Bowman (1998), Relationships of leaf dark respiration to leaf nitrogen, specific leaf area and leaf life-span: A test across biomes and functional groups, *Oecologia*, *114*, 471–482.

Reichstein, M., et al. (2003), Inverse modeling of seasonal drought effects on canopy CO_2/H_2O exchange in three Mediterranean ecosystems, *J. Geophys. Res.*, *108*(D23), 4726, doi:10.1029/2003JD003430.

Shugart, H. H., and D. C. West (1977), Development of an Appalachian deciduous forest succession model and its application to assessment of the impact of the chestnut blight, *J. Environ. Manage.*, *5*, 161–179.

Ter-Mikaelian, M. T., and M. D. Korzukhin (1997), Biomass equations for sixty-five North American tree species, *For. Ecol. Manage.*, *97*, 1–24.

Trudinger, C. M., et al. (2007), OptIC project: An intercomparison of optimization techniques for parameter estimation in terrestrial biogeochemical models, *J. Geophys. Res.*, *112*, G02027, doi:10.1029/2006JG000367.

Uppala, S., et al. (2005), The era-40 re-analysis, *Q. J. R. Meteorol. Soc.*, *131*, 2961–3012.

Urban, D. L. (1990), A versatile model to simulate forest pattern: A users guide to ZELIG version 1.0, technical report, Environ. Sci. Dep., Univ. of Va., Charlottesville.

Urbanski, S., et al. (2007), Factors controlling CO_2 exchange on timescales from hourly to decadal at Harvard Forest, *J. Geophys. Res.*, *112*, G02020, doi:10.1029/2006JG000293.

van Iersel, M. W. (2003), Carbon use efficiency depends on growth respiration, maintenance respiration, and relative growth rate: A case study with lettuce, *Plant Cell Environ.*, *26*, 1441–1449.

Villar, R., and J. Merino (2001), Comparison of leaf construction costs in woody species with differing leaf life-spans in contrasting ecosystems, *New Phytol.*, *151*, 213–226.

von Caemmerer, S., and G. D. Farquhar (1981), Some relationships between the biochemistry of photosynthesis and the gas exchange of leaves, *Planta*, *153*, 376–387.

Walko, R. L., et al. (2000), Coupled atmosphere-biophysics-hydrology models for environmental modeling, *J. Appl. Meteorol.*, *39*, 931–944.

Wang, Y.-P., R. Leuning, H. A. Cleugh, and P. A. Coppin (2001), Parameter estimation in surface exchange models using nonlinear inversion: How many parameters can we estimate and which measurements are most useful?, *Global Change Biol.*, *7*, 495–510.

Wang, Y. P., D. Baldocchi, R. Leuning, E. Falge, and T. Vesala (2007), Estimating parameters in a land-surface model by applying nonlinear inversion to eddy covariance flux measurements from eight FLUXNET sites, *Global Change Biol.*, *13*, 652–670.

Williams, M., P. A. Schwarz, B. E. Law, J. Irvine, and M. R. Kurpius (2005), An improved analysis of forest carbon dynamics using data assimilation, *Global Change Biol.*, *11*, 89–105.

Wilson, K. B., D. D. Baldocchi, and P. J. Hanson (2000), Quantifying stomatal and non-stomatal limitations to carbon assimilation resulting from leaf aging and drought in mature deciduous tree species, *Tree Physiol.*, *20*, 787–797.

Wofsy, S., et al. (1993), Net exchange of CO_2 in a mid-latitude forest, *Science*, *260*, 1314–1317.

Wright, I. J., et al. (2004), The worldwide leaf economics spectrum, *Nature*, *428*, 821–827.

Zhang, X., et al. (2003), Monitoring vegetation phenology using MODIS, *Remote Sens. Environ.*, *84*, 471–475.

D. Y. Hollinger, Northern Research Station, USDA Forest Service, 271 Mast Road, Durham, NH 03824, USA. (dhollinger@fs.fed.us)

D. Medvigy, Department of Civil and Environmental Engineering, Duke University, Box 90287, Durham, NC 27708, USA. (medvigy@post.harvard.edu)

P. R. Moorcroft, Department of Organismic and Evolutionary Biology, Harvard University, 22 Divinity Avenue, Cambridge, MA 02138, USA. (paul_moorcroft@harvard.edu)

J. W. Munger and S. C. Wofsy, Department of Earth and Planetary Sciences, Harvard University, 20 Oxford Street, Cambridge, MA 02138, USA. (jwmunger@seas.harvard.edu; steven_wofsy@harvard.edu)